

# 1 Tracing the migration of mantle CO<sub>2</sub> in gas fields and mineral water 2 springs in south-east Australia using noble gas and stable isotopes

3 Rūta Karolytė<sup>1a\*</sup>, Gareth Johnson<sup>1</sup>, Domokos Györe<sup>2</sup>, Sascha Serno<sup>1</sup>, Stephanie Flude<sup>1</sup>, Finlay M.  
4 Stuart<sup>2</sup>, Allan R. Chivas<sup>3,4</sup>, Adrian Boyce<sup>2</sup> and Stuart M.V. Gilfillan<sup>1</sup>

5 <sup>1</sup>School of GeoSciences, University of Edinburgh, James Hutton Road, Edinburgh, EH9 3FE, UK

6 <sup>2</sup>Isotope Geoscience Unit, Scottish Universities Environmental Research Centre (SUERC), East  
7 Kilbride, G75 0QF, UK

8 <sup>3</sup>GeoQuEST Research Centre, School of Earth, Atmospheric and Life Sciences, University of  
9 Wollongong, Wollongong, NSW 2522, Australia

10 <sup>4</sup>Department of Earth Sciences and Sprigg Geobiology Centre, The University of Adelaide SA 5005,  
11 Australia

12 <sup>a</sup>Current address: Department of Earth Sciences, University of Oxford, 3 S Parks Rd, Oxford OX1 3AN,  
13 UK

14 \*Author for correspondence: [ruta.karolyte@earth.ox.ac.uk](mailto:ruta.karolyte@earth.ox.ac.uk)

15 Keywords: Carbon Capture and Storage; geochemical tracing; noble gases; carbon isotopes; helium;  
16 mantle; CO<sub>2</sub> springs; solubility fractionation; Otway Basin.

## 17 Abstract

18 Geochemical monitoring of CO<sub>2</sub> storage requires understanding of both innate and introduced fluids  
19 in the crust as well as the subsurface processes that can change the geochemical fingerprint of CO<sub>2</sub>  
20 during injection, storage and any subsequent migration. Here, we analyse a natural analogue of CO<sub>2</sub>  
21 storage, migration and leakage to the atmosphere, using noble gas and stable isotopes to constrain  
22 the effect of these processes on the geochemical fingerprint of the CO<sub>2</sub>. We present the most  
23 comprehensive evidence to date for mantle-sourced CO<sub>2</sub> in south-east Australia, including well gas  
24 and CO<sub>2</sub>-rich mineral spring samples from the Otway Basin and Central Victorian Highlands (CVH).  
25 <sup>3</sup>He/<sup>4</sup>He ratios in well gases and CO<sub>2</sub> springs range from 1.21 to 3.07 R<sub>A</sub> and 1.23 – 3.65 R<sub>C</sub>/R<sub>A</sub>,  
26 respectively. We present chemical fractionation models to explain the observed range of <sup>3</sup>He/<sup>4</sup>He  
27 ratios, He, Ne, Ar, Kr, Xe concentrations and δ<sup>13</sup>C(CO<sub>2</sub>) values in the springs and the well gases. The  
28 variability of <sup>3</sup>He/<sup>4</sup>He in the well gases is controlled by the gas residence time in the reservoir and

29 associated radiogenic  $^4\text{He}$  accumulation.  $^3\text{He}/^4\text{He}$  in  $\text{CO}_2$  springs decrease away from the main  
30 mantle fluid supply conduit. We identify one main pathway for  $\text{CO}_2$  supply to the surface in the CVH,  
31 located near a major fault zone. Solubility fractionation during phase separation is proposed to  
32 explain the range in noble gas concentrations and  $\delta^{13}\text{C}(\text{CO}_2)$  values measured in the mineral spring  
33 samples. This process is also responsible for low  $^3\text{He}$  concentrations and associated high  $\text{CO}_2/{}^3\text{He}$ ,  
34 which are commonly interpreted as evidence for mixing with crustal  $\text{CO}_2$ . The elevated  $\text{CO}_2/{}^3\text{He}$  can  
35 be explained solely by solubility fractionation without the need to invoke other  $\text{CO}_2$  sources. The  
36 noble gases in the springs and well gases can be traced back to a single end-member which has  
37 suffered varying degrees of radiogenic helium accumulation and late stage degassing. This work  
38 shows that combined stable and noble gas isotopes in natural gases provide a robust tool for  
39 identifying the migration of injected  $\text{CO}_2$  to the shallow subsurface.

40

## 41 1. Introduction

42 The development of geochemical tracing techniques to ascertain the origin and genetic link  
43 between natural gases trapped in subsurface reservoirs and those degassing at the surface is  
44 important to the safe and successful deployment of carbon capture and storage (CCS). Safe disposal  
45 of captured industrial  $\text{CO}_2$  requires verification of the fate of the injected gas and reassurance that  
46 injected gas does not migrate to the surface (IPCC, 2005). To ensure this, CCS operators have to  
47 adhere to legislative guidelines and verify that injected  $\text{CO}_2$  is securely contained within the reservoir  
48 formation (Dixon et al., 2015). While a variety of geophysical, geoelectric and thermal sensing  
49 monitoring techniques exist (Giese et al., 2009), the high sensitivity of geochemical monitoring  
50 techniques is useful for detecting seepage at low concentrations, verifying gas origin and tracing the  
51 interactions between different crustal fluids (Myers et al., 2013; Stalker and Myers, 2014; Roberts et  
52 al., 2017).

53 The noble gas isotopes have previously been applied in an engineered setting to assess  $\text{CO}_2$   
54 migration, dissolution and residual trapping in reservoir pore spaces at the Cranfield  $\text{CO}_2$ -EOR site  
55 field (Györe et al., 2015; Györe et al., 2017) and to study industrial underground natural gas storage  
56 in the Paris Basin (Jeandel et al., 2010). Noble gas tracers have been used to refute allegations of  
57 injected  $\text{CO}_2$  leakage to the surface near the Weyburn-Midale  $\text{CO}_2$  Monitoring and Storage Project  
58 (Gilfillan et al., 2017) and to identify fugitive gas migration to shallow aquifers caused by industrial  
59 hydraulic fracturing operations (Darrah et al., 2014). The techniques used in these industrial studies  
60 have been informed by preceding research of natural gas fields and springs (e.g. Ballentine and

61 O’Nions, 1994; Gilfillan et al., 2014, 2009, 2008; Sherwood Lollar et al., 1997; Wilkinson et al., 2009).  
62 Natural analogue studies remain a crucial gateway to developing geochemical tracing methods for  
63 the industrial sector, providing information about fluid migration and retention processes occurring  
64 over geological time scales (Baines and Worden, 2004; Haszeldine et al., 2005; Holland and Gilfillan,  
65 2013).

66 Helium is an unrivalled indicator of crustal fluid migration in the subsurface because it is  
67 sensitive to changes in the balance between volatiles derived from the mantle and the crust. This is  
68 because the original helium composition of any subsurface fluid is not significantly modified by  
69 interaction with groundwater due to the low abundance of helium in the atmosphere (Ozima and  
70 Podosek, 2002). Hence, helium is particularly applicable to tracing gas migration through a water  
71 system in both natural and industrial fugitive gas migration monitoring settings. Here we draw from  
72 existing methodologies of helium use in tracing the migration of mantle fluids (Sano et al., 1990;  
73 Sakamoto et al., 1992), mixing of different fluid sources (O’Nions and Oxburgh, 1988; Sano and  
74 Marty, 1995) and dating natural gas and groundwater resources (Zhou and Ballentine, 2006; Liu et  
75 al., 2016) to provide a comprehensive account on the geochemical link between natural CO<sub>2</sub> gases,  
76 trapped in the subsurface and emanating in the shallow surface.

77 Noble gases are soluble in water and partition according to their relative solubilities during  
78 gas-water equilibration. This property has been utilised mainly in assessing reservoir-scale water-gas  
79 equilibration and gas migration or groundwater recharge conditions (Bosch and Mazor, 1988;  
80 Ballentine et al., 1996; Barry et al., 2016) and the presence of ‘excess air’ above the atmospheric  
81 solubility equilibrium (Aeschbach-Hertig et al., 2008; Kipfer et al., 2002). The former is largely based  
82 on atmospheric noble gas ratios, whilst the latter combines ratios with elemental concentrations.  
83 Atmospheric noble gas ratios in CO<sub>2</sub> springs are commonly similar to air saturated-water (ASW) and  
84 the utility of these noble gases is commonly overlooked. We discuss the use of noble gas  
85 concentration data in assessing the solubility fractionation effects of near-surface degassing and  
86 reconstructing the original noble gas composition for the purpose of tracing.

87 The physical and chemical processes contributing to and modifying the noble gas contents of  
88 CO<sub>2</sub> are explored using the data from three natural CO<sub>2</sub> fields in the Otway Basin of SE Australia and  
89 ten natural CO<sub>2</sub>-rich springs in Victoria. We focus on identifying the origin of the gases and the  
90 genetic link between gases stored in reservoir traps and those emanating at the surface from the  
91 natural mineral springs.

## 92 2 Geological setting

### 93 2.1 Basin setting and location of CO<sub>2</sub> gas fields and springs

94 The Otway Basin developed along the southern Australian margin as a result of crustal  
95 extension due to sea floor spreading between Australia and Antarctica. The sedimentary section of  
96 the basin comprises Upper Jurassic – Lower Cretaceous Otway Group sediments (Bernecker and  
97 Moore, 2003). The present geometry of the basin is characterised by NW-SE trending normal faults,  
98 and was established during Jurassic to Cretaceous rifting and subsequent reactivation during a short-  
99 lived period of basin inversion in the Miocene (Cox et al., 1995; Teasdale et al., 2003).

100 The basement comprises Lachlan and Delamerian fold belts, separated by the Moyston  
101 lithospheric suture which extends to the Moho (Fig. 1a). Parallel N-S trending large-scale shear zones  
102 and reverse faults connect to the Moyston Fault at depth (Fig. 1d) (Cayley et al., 2011). The structure  
103 of the Otway Basin has been strongly controlled by the fabric of the underlying basement. Old  
104 basement structures have a significant rheology contrast along them and are more likely to undergo  
105 structural reactivation during a change in the stress regime (Hand and Sandiford, 1999). The Jurassic-  
106 Cretaceous extension was mainly accommodated along structural weaknesses of the basement,  
107 which created graben and half-graben structures favourable for fluid trapping. Hydrocarbons and  
108 CO<sub>2</sub> discoveries in the Otway Basin therefore tend to coincide with the location of deep basement  
109 faults (Bernecker and Moore, 2003).

110 The basin contains numerous accumulations of CO<sub>2</sub>, methane and other hydrocarbons in  
111 varying concentrations (Boult et al., 2004). The three gas fields investigated in this work contain CO<sub>2</sub>  
112 concentrations above 75 mol %, with the remainder of the gas content being primarily methane. The  
113 Caroline field is located in South Australia, near Mt Gambier and is a commercially explored CO<sub>2</sub> field  
114 which has a CO<sub>2</sub> concentration in excess of 98 %. At reservoir depth and temperature (2.5 km, 92 °C),  
115 CO<sub>2</sub> is in a supercritical fluid phase (Chivas et al., 1987). Boggy Creek and Buttress fields are located  
116 in the Port Campbell Embayment at the eastern side of the Otway Basin. Both fields contain  
117 mixtures of CO<sub>2</sub> and methane in the gas phase with no significant liquid hydrocarbon component  
118 (Boreham et al., 2011). Methane generation is dated to mid-Paleogene (Duddy, 1997), followed by a  
119 later-stage CO<sub>2</sub> emplacement (Boult et al., 2004; Watson et al., 2004; Lyon et al., 2005).

120 CO<sub>2</sub>-rich mineral spring waters emanate at the ground surface within the extent and north of  
121 the basin. Over a hundred ambient temperature mineral springs are located in the Central Victorian  
122 Highlands (CVH) (Fig. 1b). Mineral water flows through a fracture-dominated aquifer consisting of  
123 Ordovician low-grade metasedimentary sequence and discharges into topographic lows such as

124 streambeds. Many of the springs also release CO<sub>2</sub> and can be identified as degassing CO<sub>2</sub> bubble  
125 trails into creek beds or standing pools of water. Springs are clustered along the Muckleford Fault,  
126 which is a deep Proterozoic reverse fault extending down to the lower crust and connecting to the  
127 Moyston suture zone (Cayley et al., 2011) (Fig. 1d).

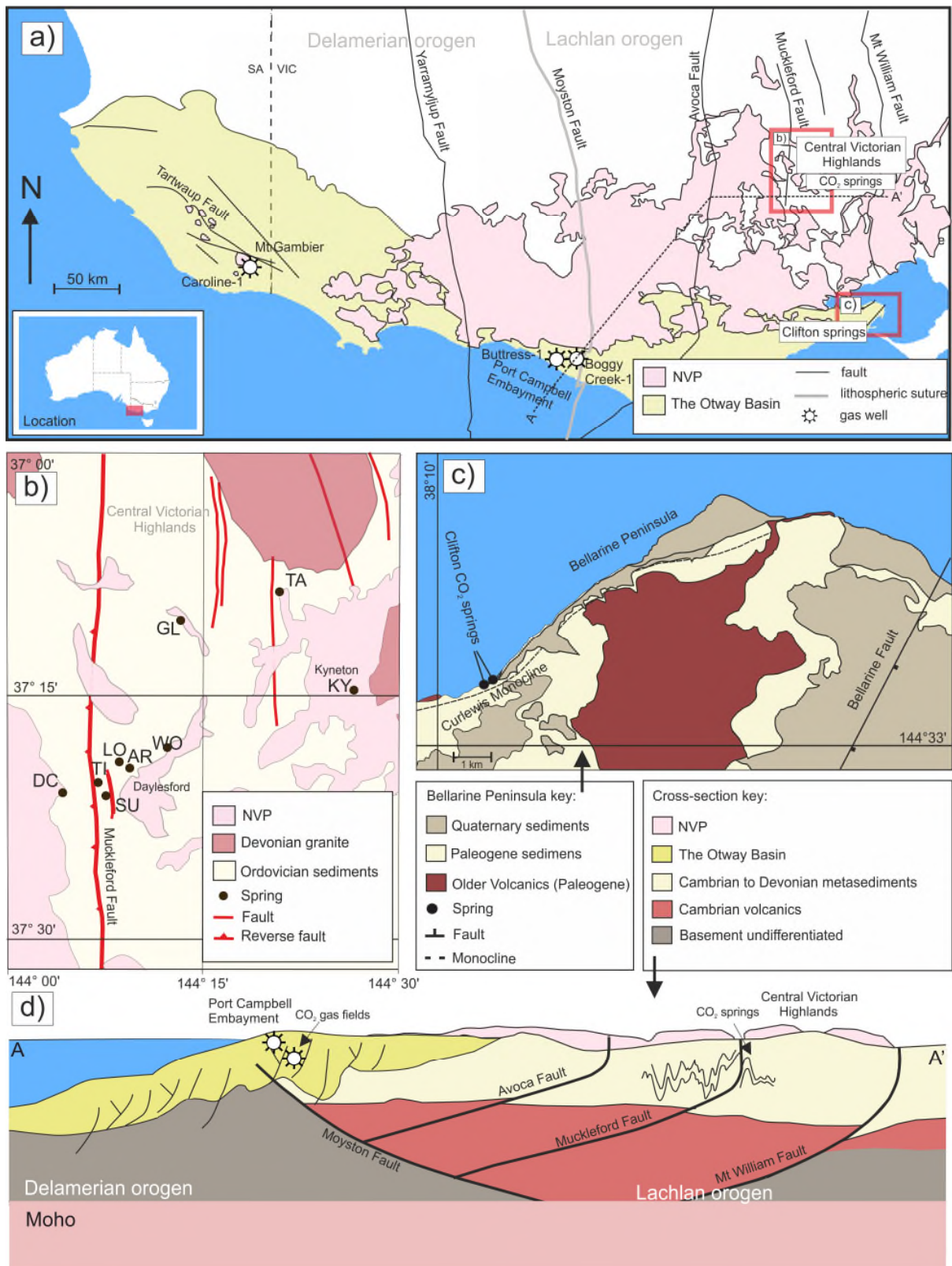
128 Mineral springs also emerge on the northern coast of Bellarine Peninsula, at Clifton Springs  
129 near Geelong, on the south-eastern edge of the Otway Basin (Fig. 1c). The central part of the  
130 Bellarine Peninsula has been uplifted in the late Miocene during the inversion of NE-SW trending  
131 normal faults (Coulson, 1933). The north coast of the peninsula is structurally controlled by the  
132 Curlewis Monocline, underlain by a south dipping normal fault. The Curlewis Monocline is parallel to  
133 the structural lineaments of the basement and could be associated with deeper basement faults  
134 (Dahlhaus, 2003). CO<sub>2</sub> springs emerge along the shoreline parallel to the fault.

135 The basement and the Otway Basin are overlain by the Newer Volcanic Province (NVP)  
136 extrusives that stretch from the CVH to the northern edges of the Port Campbell Embayment. The  
137 province is a well preserved intra-plate basaltic lava field with more than 400 eruptive centres  
138 (Boyce, 2013), active between 5 Ma and 4.5 ka (Cas et al., 2017). The last eruption dated at 4.5 ka,  
139 occurred at Mount Gambier, located near the Caroline CO<sub>2</sub> field (Robertson et al., 1996). Many of  
140 the oldest eruptive centres are found in the eastern side of the province and near the CVH (4.6 - 2.6  
141 Ma) (Price et al., 1997), but no systematic pattern of eruption ages exists (Cas et al., 2017). There is  
142 no evidence for volcanic activity of this period in the Bellarine Peninsula where Clifton Springs are  
143 located, although The Older Volcanics (39 - 49 Ma) crop out in the area (Price et al., 1997). The cause  
144 of the recent volcanism is currently unresolved. Common theories include a mantle plume (Wellman  
145 and McDougall, 1974; Wellman, 1983), edge-driven isolated mantle convection (King and Anderson,  
146 1998), batch-melting caused by fault reactivation (Lesti et al., 2008), or a combination of all these  
147 factors (Demidjuk et al., 2007; Davies and Rawlinson, 2014).

## 148 2.2 Previous noble gas studies of the gas fields and CO<sub>2</sub> springs

149 Despite the commercial exploration of CO<sub>2</sub> gas fields in the Otway Basin and springs in the  
150 CVH, studies of the CO<sub>2</sub> origins have been limited and the processes associated with the gas  
151 migration in the subsurface and to the surface are poorly understood. MORB and solar noble gas  
152 signatures have been identified in mantle xenolith samples from the Newer Volcanics (Matsumoto et  
153 al., 1997, 2002), primarily within CO<sub>2</sub>-rich fluid inclusions (Matsumoto et al., 1998). Chivas et al.  
154 (1987) reported <sup>3</sup>He/<sup>4</sup>He values of up to 3.1 R<sub>A</sub> in the Caroline field and Caffee et al. (1999) identified  
155 the presence of primordial Xe in the field, providing evidence for a mantle source. Mantle helium has

156 also been reported in the Lavers-1 gas field in the Otway Basin (1.68 R/R<sub>A</sub>) (Watson et al., 2004).  
157 Preliminary <sup>3</sup>He/<sup>4</sup>He measurements of up to 3.1 R<sub>A</sub> have been reported in CO<sub>2</sub> springs at the CVH  
158 (Chivas et al., 1983) but no further study has been published. It has been suggested that the source  
159 of mantle volatiles in CO<sub>2</sub> springs is associated with the NVP (Lawrence, 1969), however no  
160 conclusive evidence currently exists other than geographic proximity to the eruptive centres. Prior to  
161 this work no geochemical study into the origin of the CO<sub>2</sub> degassing at the Bellarine Peninsula had  
162 been published.



163  
 164 **Figure 1.** Location map of the studied CO<sub>2</sub> gas fields and springs. **a)** Studied well gases are in two localities in the Otway  
 165 Basin: Port Campbell Embayment and Mt Gambier. Clifton Springs are located on the eastern edge of the basin. The CVH  
 166 CO<sub>2</sub> springs emerge from the Ordovician basement rocks in the CVH (Central Victorian Highlands). The Otway Basin and  
 167 CVH are dissected by N-S trending faults. The NVP (Newer Volcanic Province) extends across both areas. **b)** Location of  
 168 sampled CO<sub>2</sub> springs in CVH; many of the springs are located near the Muckleford Fault (see Table 1 for sample name  
 169 abbreviations). **c)** Clifton Springs are located on the coast of Bellarine Peninsula, along the crest of the Curlewis

170 **Monocline. d) Sketch cross-section (not to scale) of A-A' transect on Fig. 1a, showing the structural relationship between**  
171 **the basement and the basin. The Moyston and Mt Williams Faults extend to the Moho. Many of the basement faults**  
172 **(including The Muckelford fault at CVH) are inferred to be connected to the Moyston Fault at depth. Elements of the**  
173 **figure adapted from** (Cartwright et al., 2002; Bernecker and Moore, 2003; Watson et al., 2003; Cayley et al., 2011; Cas et  
174 al., 2017).

## 175 2. Methods

### 176 2.1 Gas sampling

177 The reported samples are in two distinct groups: 'well samples' refer to produced gases  
178 collected from well heads. 'Spring samples' refer to sample collected at water pools and streams  
179 where CO<sub>2</sub> is naturally degassing. Gas samples from the natural gas fields in the Otway Basin were  
180 collected directly from producing well heads, using 9.5 mm diameter refrigeration grade copper  
181 tubing connected to a pressure regulator by plastic hosing. Bubbling gases from the springs were  
182 collected using an inverted plastic funnel placed over a bubbling vent, placed into the water column  
183 to form an air-tight seal, allowing gas to flow through plastic hose to the copper tube. Tubes were  
184 purged for 5 minutes and sealed using two steel clamps specifically manufactured for the purpose of  
185 creating a helium leak-tight cold weld seal (Holland and Gilfillan, 2013). Mineral spring water  
186 samples were collected via hand pumps, filtered through 0.45 µm pore-size filters and filled into  
187 Nalgene bottles. The temperature, pH and TDS of the water in shallow tube bores was measured in  
188 the field using a Hanna Instruments HI991300 Portable Waterproof temperature/pH/EC Meter with  
189 an accuracy of ± 0.5 °C, ± 0.01 pH and ± 1 µS/cm for temperature, pH and electrical conductivity  
190 respectively. TDS values were obtained from EC measurements using a conversion factor of 0.7  
191 (Walton, 1989).

### 192 2.2 Laboratory procedures

193 All laboratory work was undertaken at the Scottish Universities Environmental Research  
194 Centre (SUERC). Copper tube samples were connected to an all-metal vacuum line, purified using VG  
195 Scienta ST22 titanium sublimation pump and ZrAl alloy getter. The isotopic composition of noble  
196 gases was measured using a MAP 215-50 mass spectrometer using techniques outlined in Györe et  
197 al. (2015). Bulk gas concentrations were measured using a Pfeiffer Vacuum QMS 200 quadrupole  
198 mass spectrometer and Hewlett Packard 5890 Series 11 Gas Chromatograph with uncertainties of ±1  
199 %. Major gas concentrations are reported corrected for air. δ<sup>13</sup>(CO<sub>2</sub>) values were determined using a  
200 VG Optima dual inlet isotope ratios mass spectrometer in dynamic mode using an internal standard  
201 (Dunbar et al., 2016). Values are reported relative to VPDB standard with uncertainties of ±0.2 ‰.



### 202            3. Results

203            A total of three well gas and ten spring samples were measured. Sample location, bulk gas  
204 composition,  $\delta^{13}(\text{CO}_2)$  values, temperature, pH and TDS measurements are reported in Table 1. He,  
205 Ne and Ar isotope ratios, and He, Ne, Ar, Kr, Xe concentrations are reported in Table 2. The full suite  
206 of noble gases was measured in six of the  $\text{CO}_2$  spring samples, while only He and Ne isotopes were  
207 measured in three well gas and four  $\text{CO}_2$  spring samples.

208 **Table 1. Details of the geographic location, bulk gas composition,  $\delta^{13}\text{C}(\text{CO}_2)$  values of 3 well gases and 10  $\text{CO}_2$  springs; pH, temperature and TDS measured in water from**  
 209 **10 mineral water bores.**

Sample name	Label	Location			Bulk gas composition*							$\delta^{13}\text{C}(\text{CO}_2)$	Water from shallow bores		
		Region	Latitude	Longitude	$\text{CO}_2$	$\text{CH}_4$	$\text{C}_2\text{H}_6$	$\text{C}_3\text{H}_8$	$\text{C}_4\text{H}_{10}$	$\text{N}_2$	VPDB	pH	T °C	TDS g/L	
<i>Well gases</i>															
<b>Caroline-1</b>	<b>CA</b>	Mount Gambier, SA	-37.9417	140.9083	99	0.9	0.01	–	–	0.4	-4.1	–	–	–	
<b>Boggy Creek-1</b>	<b>BC</b>	Port Campbell, VIC	-38.5261	142.8245	87	10.0	0.1	0.03	0.01	2.3	-5.6	–	–	–	
<b>Buttress-1</b>	<b>BU</b>	Port Campbell, VIC	-38.5167	142.8084	77	19.7	0.8	1.1	–	1.9	-7.6	–	–	–	
<i>CO<sub>2</sub> springs</i>															
<b>Taradale</b>	<b>TA</b>	CVH	-37.1393	144.3500	>99						-9.4	6.1	20.9	2.9	
<b>Locarno</b>	<b>LO</b>	CVH	-37.3113	144.1412	>99						-7.2	6.1	16.7	1.6	
<b>Deep Creek</b>	<b>DC</b>	CVH	-37.3419	144.0733	>99						-8.2	5.6	15.7	0.6	
<b>Glenluce</b>	<b>GL</b>	CVH	-37.1623	144.2225	>99	0.1					-7.8	6.3	16.7	2.2	
<b>Woolnoughs</b>	<b>WO</b>	CVH	-37.2942	144.2065	>99						-6.9	6.2	21.1	1.6	
<b>Clifton Springs</b>	<b>CS</b>	Bellarine Peninsula	-38.1510	144.5659	>99						-6.0	5.5	20.5	3.8	
<b>Sutton</b>	<b>SU</b>	CVH	-37.3480	144.1317	>99						-8.4	6.0	19.7	1.1	
<b>Argyle</b>	<b>AR</b>	CVH	-37.3141	144.1553	>99						-9.2	5.8	15.1	1.0	
<b>Kyneton</b>	<b>KY</b>	CVH	-37.2358	144.4200	>99						-8.0 <sup>a</sup>	6.1	18.3	1.2	
<b>Tipperary</b>	<b>TI</b>	CVH	-37.3391	144.1186	>99						-7.1	6.3	16.5	2.2	

210 \* Bulk gas composition for Caroline-1 from Chivas et al. (1987), Boggy Creek-1 from Akbari (1992)

211 <sup>a</sup> from Cartwright et al. (2002)

212 Table 2. Noble gas concentrations and isotopic ratios for 3 well gas samples and 10 CO<sub>2</sub> springs.

Sample name	<sup>3</sup> He/ <sup>4</sup> He (R <sub>C</sub> /R <sub>A</sub> )	<sup>20</sup> Ne/ <sup>22</sup> Ne	<sup>21</sup> Ne/ <sup>22</sup> Ne	<sup>40</sup> Ar/ <sup>36</sup> Ar	<sup>38</sup> Ar/ <sup>36</sup> Ar	<sup>4</sup> He x 10 <sup>-6</sup>	<sup>20</sup> Ne x 10 <sup>-9</sup>	<sup>40</sup> Ar x 10 <sup>-5</sup>	<sup>84</sup> Kr x 10 <sup>-9</sup>	<sup>132</sup> Xe x 10 <sup>-10</sup>
<i>Well gases</i>										
<b>Caroline-1</b>	3.07 (0.12)	–	–	–	–	96.0 (5.0)	2.2 (0.1)	–	–	–
<b>Boggy Creek-1</b>	1.21 (0.01)	–	–	–	–	384.4 (18.6)	124.1 (5.3)	–	–	–
<b>Buttress-1</b>	1.25 (0.01)	–	–	–	–	478.8 (23.2)	15.4 (0.7)	–	–	–
<i>CO<sub>2</sub> springs</i>										
<b>Taradale</b>	1.23 (0.03)	9.73 (0.06)	0.030 (0.001)	314 (1)	0.195 (0.008)	4.0 (0.2)	34.3 (1.5)	5.3 (0.2)	8.2 (0.3)	6.9 (0.4)
<b>Locarno</b>	3.14 (0.09)	9.68 (0.05)	0.030 (0.001)	303 (1)	0.191 (0.003)	5.7 (0.2)	59.1 (2.5)	7.8 (0.3)	10.4 (0.43)	6.5 (0.3)
<b>Deep Creek</b>	2.45 (0.07)	9.92 (0.05)	0.029 (0.001)	301 (5)	0.190 (0.003)	8.9 (0.4)	132.3 (5.6)	22.8 (0.8)	39.5 (1.6)	30.4 (1.6)
<b>Glenluce</b>	1.57 (0.07)	9.71 (0.05)	0.028 (0.000)	308 (1)	0.189 (0.003)	163.0 (6.0)	1372 (58)	94.4 (3.5)	63.1 (2.6)	25.6 (1.3)
<b>Woolnoughs</b>	1.71 (0.07)	9.78 (0.06)	0.030 (0.001)	299 (1)	0.190 (0.003)	0.97 (0.04)	1781 (3.7)	86.0 (3.2)	79.9 (3.3)	36.1 (1.9)
<b>Clifton Springs</b>	1.97 (0.06)	9.73 (0.06)	0.029 (0.001)	323 (1)	0.191 (0.003)	42.0 (2.0)	128.8 (5.5)	22.9 (0.8)	29.8 (1.2)	19.9 (1.0)
<b>Sutton</b>	3.14 (0.03)	–	–	–	–	1.61 (0.05)	42.5 (1.5)	–	–	–
<b>Argyle</b>	3.65 (0.08)	–	–	–	–	87.9 (2.6)	5502 (196)	–	–	–
<b>Kyneton</b>	1.24* (0.04)	–	–	–	–	4.9 (0.1)	13834 (493)	–	–	–
<b>Tipperary</b>	2.70 (0.05)	–	–	–	–	0.48 (0.01)	438.3 (8.9)	–	–	–

213 Concentrations are in cm<sup>3</sup>(STP)/cm<sup>3</sup>. Standard conditions are 0 °C at 1 bar.

214 Errors are 1σ standard deviation.

215 \* <sup>3</sup>He/<sup>4</sup>He reported uncorrected for atmospheric component due to air contamination

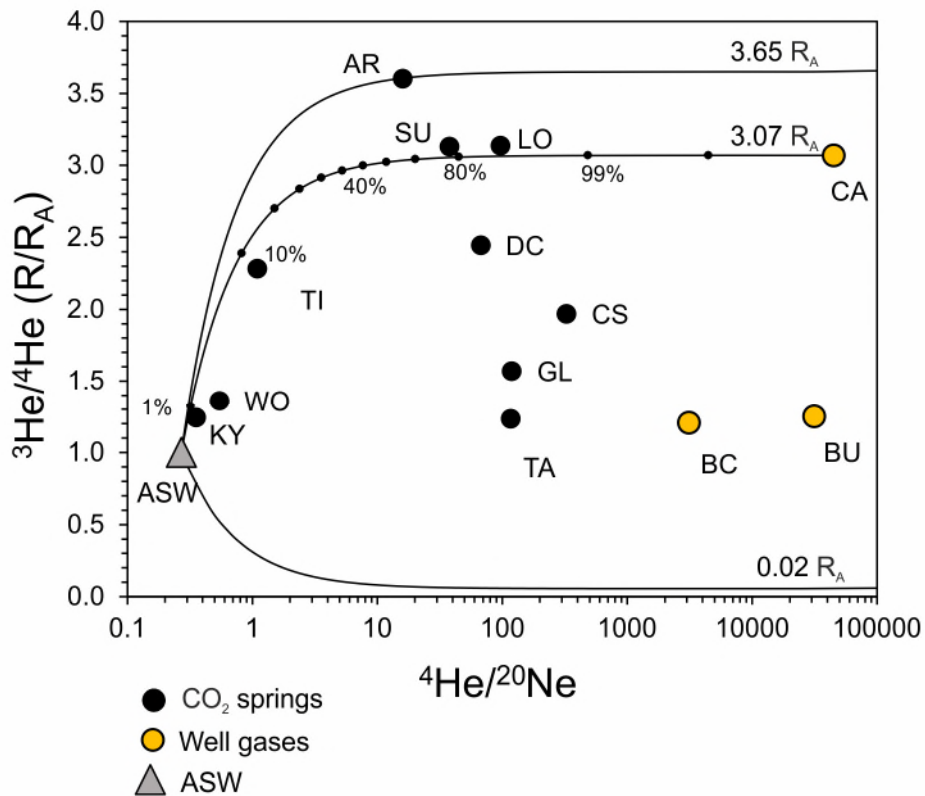
### 216 3.1. Bulk gas concentrations, $\delta^{13}(\text{CO}_2)$ and water measurements

217 The concentration of  $\text{CO}_2$  in the Buttress field is 77 % with the remainder of gas predominately  
218 constituting of  $\text{CH}_4$  (19.7 %),  $\text{N}_2$  (1.9 %) and traces of higher hydrocarbons (0.8 %  $\text{C}_2\text{H}_6$ , 1.1 %  $\text{C}_3\text{H}_{10}$ ).  
219 Bulk gas compositions for the other two well gases are taken from the literature.  $\text{CO}_2$  concentration  
220 in the adjacent Boggy Creek field is slightly higher (87%) (Akbari, 1992). The Caroline field has the  
221 highest  $\text{CO}_2$  concentrations of 99 % with traces of  $\text{CH}_4$ ,  $\text{N}_2$  and  $\text{C}_2\text{H}_6$  (Chivas et al., 1987). All mineral  
222 spring gas samples were measured to be above 99 %  $\text{CO}_2$  with the remainder of gas composed of  
223 noble gases. Glenluce is the only spring showing trace amounts of  $\text{CH}_4$  (0.1 %). The  $\delta^{13}(\text{CO}_2)$  values of  
224 the gas samples range from -9.4 to -6 ‰ in springs, and -7.6 to -4.1 ‰ in the well gases. The  
225 temperature of the water samples varies from 15.1 – 20.9 °C, pH ranges from 5.6 to 6.3 in CVH  
226 springs and 5.5 in Clifton Springs. Total dissolved solids (TDS) values range from 0.63 to 2.85 g/L.

### 227 3.2. Noble gas results

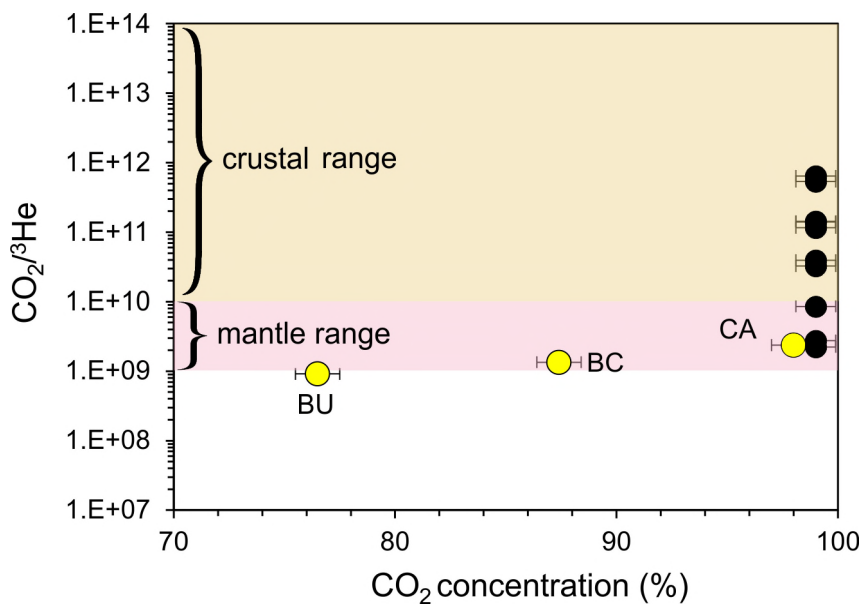
228  $^3\text{He}/^4\text{He}$  ratios are reported normalised to the value of air (where 1  $R_A$  is the atmospheric ratio  
229 of  $1.4 \times 10^{-6}$ ).  $^3\text{He}/^4\text{He } R_c/R_A$  are corrected for  $^4\text{He}$  derived from the atmospheric component, using  
230 the  $^4\text{He}/^{20}\text{Ne}$  value of the sample following the methodology in Craig (1978). It is assumed that all  
231  $^{20}\text{Ne}$  is derived from ASW and the  $^4\text{He}/^{20}\text{Ne}$  value of ASW at 20 °C is 0.27 (Kipfer et al., 2002).  
232  $^4\text{He}/^{20}\text{Ne}$  ratios of the well gases are 4-5 orders of magnitude above the ASW value (3097-44656)  
233 and range between 0.35 and 326 in the spring samples.  $^3\text{He}/^4\text{He } R_c/R_A$  values differ significantly from  
234 the measured  $^3\text{He}/^4\text{He}$  ratios in spring samples with  $^4\text{He}/^{20}\text{Ne}$  ratios <10 (Woolnoughs and  
235 Tipperary). Kyneton is the only sample with significant atmospheric contamination ( $^4\text{He}/^{20}\text{Ne} = 0.35$ )  
236 which would make the correction erroneous (Sano et al., 2006) therefore its  $^3\text{He}/^4\text{He}$  value is  
237 reported uncorrected (1.24  $R_A$ ). The  $^3\text{He}/^4\text{He}$  ratios of the remaining spring samples range from 1.23  
238 to 3.65  $R_c/R_A$ .  $^3\text{He}/^4\text{He}$  ratios of well gases from the Port Campbell region are 1.21 and 1.25  $R_A$ . The  
239 sample collected from the Caroline  $\text{CO}_2$  field in South Australia exhibits a higher value of 3.07  $R_A$ , in  
240 agreement with previous measurements (Chivas et al., 1987). All samples are compatible with two-  
241 component mixing in a  $^3\text{He}/^4\text{He}$  vs  $^4\text{He}/^{20}\text{Ne}$  plot, where variable  $^3\text{He}/^4\text{He}$  end-members mix with  
242 ASW (Fig. 2).

243  $\text{CO}_2/^3\text{He}$  ratios of the well gases are within or below the Mid-Ocean Ridge Basalt (MORB)  
244 range of  $1 \times 10^9$  to  $1 \times 10^{10}$  (Marty and Jambon, 1987). This is quite distinct from the higher  $\text{CO}_2/^3\text{He}$   
245 values predicted for near  $^3\text{He}$ -free carbonates (O'Nions and Oxburgh, 1988; Sherwood Lollar et al.,  
246 1997).  $\text{CO}_2$  concentrations in the spring samples are uniform, whilst  $\text{CO}_2/^3\text{He}$  ratios vary over two  
247 orders of magnitude,  $2.26 \times 10^9$  and  $6.5 \times 10^{11}$ , across the typical mantle and crustal values (Fig. 3).



248

249 Figure 2.  $^3\text{He}/^4\text{He}$   $R_A$  plotted against  $^4\text{He}/^{20}\text{Ne}$  ratios of springs and well gases. Solid lines depict binary  
 250 mixing between ASW and the highest regional end-member (Argyle, 3.65  $R_A$ ), Caroline field and a crustal  
 251 end-member (0.02  $R_A$ ). Black tick marks show percentage of helium from Caroline end-member in the  
 252 mixture. Few springs fall close to the mixing line with the Caroline field, the remaining samples have  
 253 variable amounts of crustal component. The errors are smaller than the symbols. Abbreviations of sample  
 254 names are given in Table 1.



255

256 **Figure 3. CO<sub>2</sub>/<sup>3</sup>He ratios plotted against CO<sub>2</sub> concentrations for the well gases (yellow circles) and CO<sub>2</sub>**  
257 **springs (black circles). The shaded area shows the range of CO<sub>2</sub>/<sup>3</sup>He values in the mantle (Marty and**  
258 **Jambon, 1987) and crustal (O’Nions and Oxburgh, 1988) sourced volatiles. Well gas samples are within the**  
259 **mantle range but with positive correlation between CO<sub>2</sub>/<sup>3</sup>He ratios and CO<sub>2</sub> concentrations. CO<sub>2</sub>**  
260 **concentrations are uniform in the spring samples, however CO<sub>2</sub>/<sup>3</sup>He ratios are wide-ranging across the**  
261 **typical mantle and crustal values. Vertical errors are smaller than symbols. Abbreviations of sample names**  
262 **are given in Table 1.**

263 Neon, argon, krypton and xenon concentrations were measured in six CO<sub>2</sub> spring samples  
264 (Taradale, Locarno, Deep Creek, Glenluce, Woolnoughs and Clifton Springs) (Table 2). <sup>20</sup>Ne/<sup>22</sup>Ne  
265 ratios of the spring samples range between 9.68 ± 0.05 and 9.92 ± 0.05, close the air value of 9.8  
266 (Eberhardt et al., 1965). <sup>40</sup>Ar/<sup>36</sup>Ar ratios range from 299 ± 1 to 323 ± 1, slightly above the value of air  
267 (298.5) (Lee et al., 2006). In contrast to relatively uniform and air-like isotope ratios, noble gas  
268 concentrations are highly variable. <sup>20</sup>Ne concentrations vary over three orders of magnitude (3.43 ±  
269 0.15 × 10<sup>-8</sup> to 1.4 ± 0.1 × 10<sup>-5</sup>); <sup>40</sup>Ar concentrations vary from 5.3 ± 0.2 × 10<sup>-5</sup> to 9.44 ± 0.43 × 10<sup>-4</sup>. <sup>84</sup>Kr  
270 and <sup>132</sup>Xe concentrations range from 8.2 ± 0.3 × 10<sup>-9</sup> to 7.9 ± 3 × 10<sup>-8</sup> and 6.5 ± 0.3 × 10<sup>-10</sup> to 3.6 ± 0.2  
271 × 10<sup>-9</sup>, respectively.

## 272 4. Discussion – link between the CO<sub>2</sub> source in the reservoirs and 273 springs

### 274 4.1. He-CO<sub>2</sub> abundance system

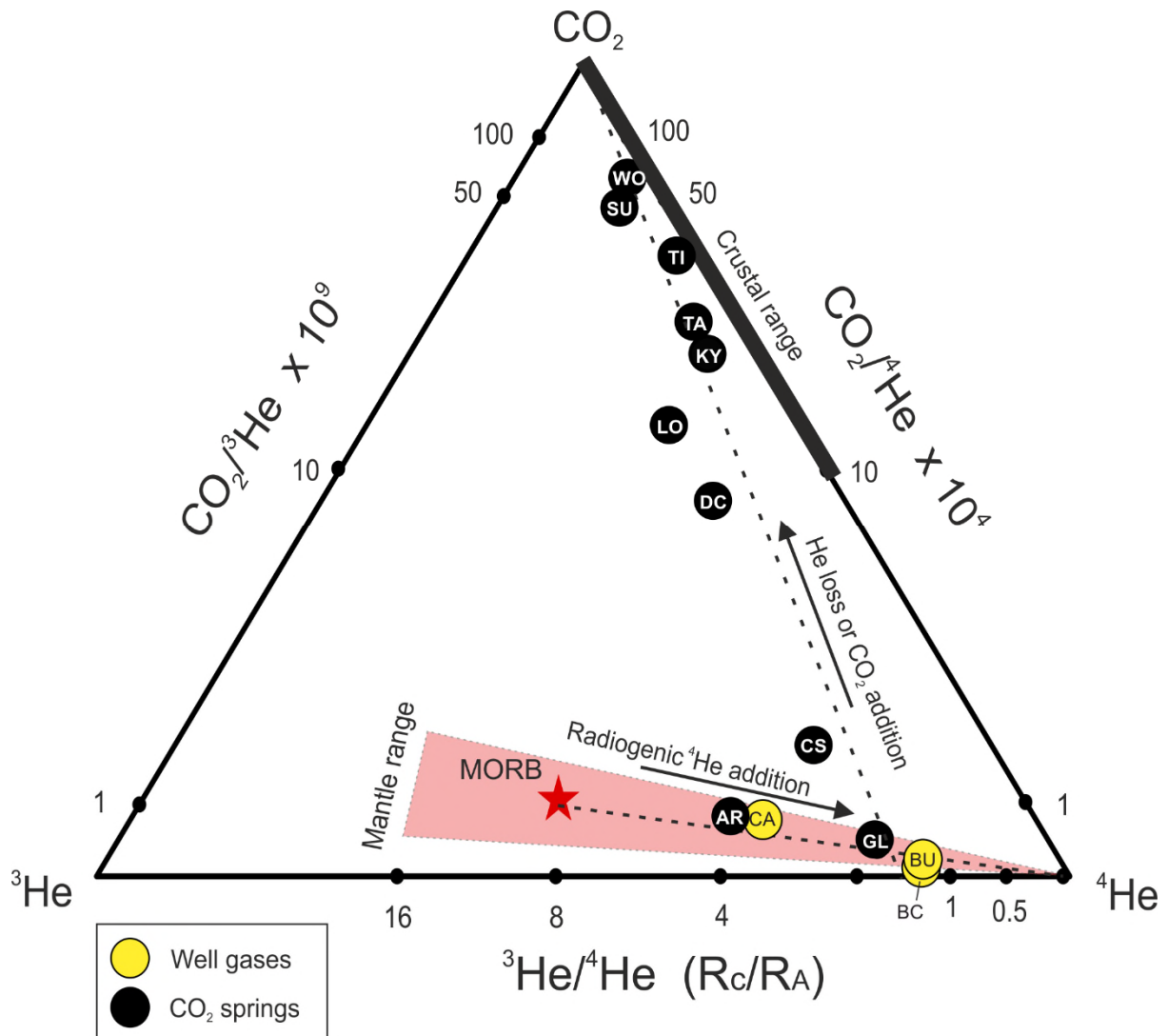
275 The trends in He-CO<sub>2</sub> abundance of well gases and CO<sub>2</sub> springs can be distinguished using a  
276 ternary diagram after Giggenbach et al. (1993). This allows depiction of the relative ratios between  
277 CO<sub>2</sub>-<sup>3</sup>He-<sup>4</sup>He rather than absolute concentrations (Fig. 4). The MORB end-member (Marty and  
278 Jambon, 1987) is displayed for reference with a straight mixing line showing addition of radiogenic  
279 <sup>4</sup>He. Caroline, Buttress, and Boggy Creek well gases as well as Argyle and Glenluce springs fall on a  
280 mixing line between MORB and crustal end-members. The rest of the springs lie on the mixing  
281 trajectory with low He/high CO<sub>2</sub> end-member (the CO<sub>2</sub> apex of the plot).

282 Based on the observed trends, two main processes can be identified. Addition of radiogenic  
283 <sup>4</sup>He to the MORB-type component lowers the <sup>3</sup>He/<sup>4</sup>He, decreases CO<sub>2</sub>/<sup>4</sup>He and does not affect  
284 CO<sub>2</sub>/<sup>3</sup>He ratio (the trend towards the <sup>4</sup>He apex of the graph). All CO<sub>2</sub> well gas and spring samples  
285 exhibit variation in <sup>3</sup>He/<sup>4</sup>He ratios due to radiogenic <sup>4</sup>He addition. Subsequently, either helium loss or  
286 CO<sub>2</sub> addition increases both CO<sub>2</sub>/<sup>3</sup>He and CO<sub>2</sub>/<sup>4</sup>He but does not affect the <sup>3</sup>He/<sup>4</sup>He ratios. The second

287 process affects the majority of the springs (excluding Glenluce and Argyle) but none of the well gas  
288 samples (trajectory towards the CO<sub>2</sub> apex of the plot).

289 To evaluate this two-step process in the following discussion, we select two samples to use as  
290 initial end-members. Argyle spring is representative of the regional high-mantle end member, least  
291 affected by radiogenic <sup>4</sup>He addition (exhibiting the highest measured <sup>3</sup>He/<sup>4</sup>He ratio 3.65 of R<sub>c</sub>/R<sub>A</sub>,  
292 [<sup>4</sup>He] = 8.8 ± 0.3 × 10<sup>-5</sup> cm<sup>3</sup>(STP)/cm<sup>3</sup>). The highest He concentrations were measured in Glenluce  
293 sample (<sup>3</sup>He/<sup>4</sup>He 1.57 R<sub>c</sub>/R<sub>A</sub>, [<sup>4</sup>He]=1.6 ± 0.1 × 10<sup>-4</sup> cm<sup>3</sup>(STP)/cm<sup>3</sup>), which is the least affected by  
294 secondary He loss or CO<sub>2</sub> addition.

295 The <sup>3</sup>He/<sup>4</sup>He ratio can be modified by dilution with non-CO<sub>2</sub> gas (usually methane) with a  
296 different He isotopic signature (Sherwood Lollar et al., 1994), radiogenic <sup>4</sup>He accumulation in situ  
297 (Newell et al., 2015; Liu et al., 2016) or He stripping from formation water during gas migration  
298 through lithological units enriched in <sup>4</sup>He (Sano et al., 1990; Sakamoto et al., 1992). The resulting  
299 <sup>3</sup>He/<sup>4</sup>He ratio can then be overprinted by addition of CO<sub>2</sub> from a different source (O'Nions and  
300 Oxburgh, 1988) or phase fractionation during degassing (Matthews et al., 1987). If the well gases  
301 and CO<sub>2</sub> springs share a common source, then these processes can be accounted for and gas  
302 composition can be traced back to a single initial end-member.



303

304

305

306

307

308

309

310

Figure 4. Ternary diagram (after Giggenbach et al., 1993) showing the relationship between the concentrations of CO<sub>2</sub>, <sup>3</sup>He, <sup>4</sup>He expressed as their ratios. MORB value used for reference is 8 ± 1 R<sub>A</sub> (Marty and Jambon, 1987). The dashed lines show mixing between different components. The two clear trends are: 1) Radiogenic <sup>4</sup>He addition, which shifts gas composition to the right apex of the ternary plot, 2) CO<sub>2</sub> addition or He loss trend towards the top apex of the plot. Port Campbell well gases fall on the mixing line between MORB and crustal end-member. Spring samples fall on He loss/CO<sub>2</sub> addition trendline. Abbreviations of sample names are given in Table 1.

311

#### 4.2 Radiogenic <sup>4</sup>He addition

312

313

314

315

316

<sup>4</sup>He is produced by the alpha decay of uranium and thorium in the crust. These elements are primarily concentrated in accessory minerals such as zircon and apatite, which release helium at a constant rate above the blocking temperature of the mineral (Tolstikhin et al., 2017). Similarly, <sup>3</sup>He is produced by thermal neutron capture by <sup>6</sup>Li, which can be approximated based on Li content of the crust (Ballentine and Burnard, 2002). However, this contribution is minimal relative to the amount of



317 <sup>3</sup>He released from mantle fluids and can be considered to be negligible in the context of in-situ  
318 crustal helium accumulation.

319 After production, radiogenic helium is either trapped in the pore spaces in-situ or mobilised by  
320 any migrating water or gas phase present in the subsurface and then transported elsewhere. If a  
321 natural gas trap exists in-situ, helium will preferentially accumulate in the gas phase due to its low  
322 solubility in water.

#### 323 4.2.1. Radiogenic <sup>4</sup>He accumulation in-situ

324 The initial <sup>3</sup>He/<sup>4</sup>He ratio of mantle-sourced gas can be reduced by direct accumulation of <sup>4</sup>He  
325 produced in the crust, or by mixing with <sup>4</sup>He-rich methane. The former would be applicable to CO<sub>2</sub>  
326 springs, the latter to well gases containing CO<sub>2</sub> and CH<sub>4</sub> mixtures. In both cases, the final <sup>4</sup>He  
327 concentrations are controlled by the rate of <sup>4</sup>He production in the crust. The contents of radiogenic  
328 <sup>4</sup>He accumulated in-situ in a natural gas trap can therefore be considered as a function of time since  
329 the initial emplacement of the gas in the trap, given a known crustal helium production rate (Liu et  
330 al., 2016). Under this assumption, we can estimate the residence time required for the observed  
331 <sup>3</sup>He/<sup>4</sup>He ratios in both the well gases and the springs.

332 The <sup>4</sup>He production rate (Craig and Lupton, 1976) and <sup>4</sup>He concentration in the pore fluid  
333 increases at the rate of  $J_{He}$  (Torgersen, 1980):

$$334 \quad {}^4P = 0.2355 \times 10^{-12} \times [U] \times (1 + 0.123 \times [Th]/[U] - 4) \quad (1)$$

$$335 \quad J_{He} = {}^4P \times \rho \times (1 - \phi)/\phi \quad (2)$$

336 Where:

337 [U], [Th] – concentrations in ppm

338 <sup>4</sup>P – crustal <sup>4</sup>He production rate in cm<sup>3</sup>STP/g yr

339  $J_{He}$  – <sup>4</sup>He production rate cm<sup>3</sup>STP/yr

340  $\rho$  – density of the crust in g/cm<sup>3</sup>

341  $\phi$  – porosity of the rocks as a fraction

342 Assuming <sup>4</sup>He has been accumulating in mantle-sourced CO<sub>2</sub> with a known initial composition,  
343 the final <sup>3</sup>He/<sup>4</sup>He ratio is expressed as a function of time modified from Newell et al. (2015):

344  ${}^3\text{He}/{}^4\text{He}(t) = F \times {}^3\text{He}_m / (J_{\text{He}} \times t + \times {}^4\text{He}_m)$  (3)

345 Where:

346  $F$  – fraction of mantle-sourced gas in the reservoir

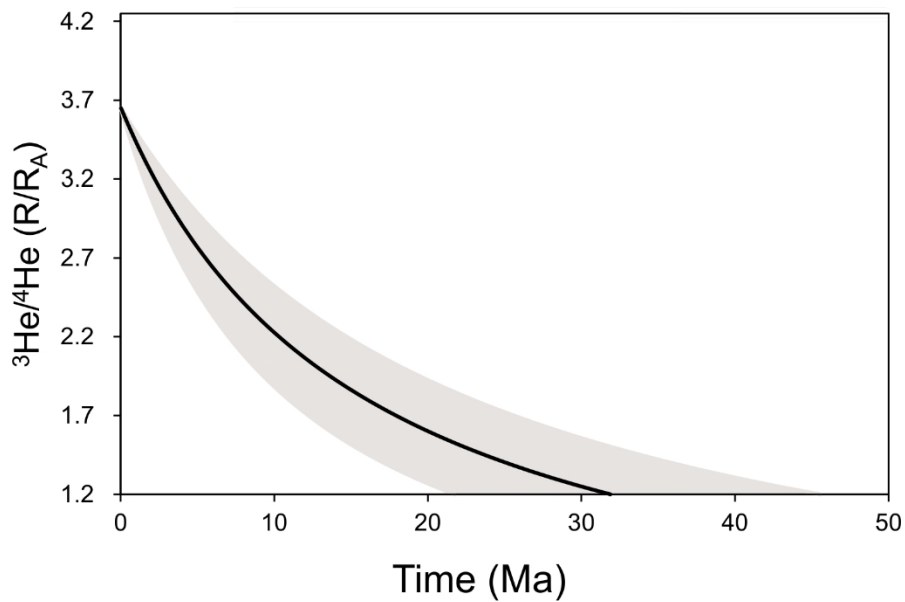
347  $\text{He}_m$  – helium concentration of the mantle-source end-member

348  $t$  – time in years

349 The final result is independent of the timing of CO<sub>2</sub> emplacement as it records the total <sup>4</sup>He  
350 accumulated since the start of the gas trap filling, so in the case of CO<sub>2</sub>/methane mixture, the  
351 recorded age will be that of the methane emplacement. Argyle spring concentrations are taken as  
352 representative of the initial mantle-sourced end-member, based on the highest measured <sup>3</sup>He/<sup>4</sup>He  
353 ratio (3.65 R<sub>c</sub>/R<sub>A</sub>). This ratio is significantly lower than SCLM or MORB values, but we assume this to  
354 be representative of the end-member at the time of emplacement. Similar value is measured in the  
355 Caroline field which has likely been emplaced at a similar time to Mount Gambier eruptions dated at  
356 5 ka (Roberston et al., 1996), so we assume this to be a regional feature and that some radiogenic  
357 <sup>4</sup>He accumulation occurred within the melt before the gas emplacement.

358 Assuming an average reservoir porosity of 25 % (Watson et al., 2003), average crustal <sup>238</sup>U and  
359 <sup>232</sup>Th concentrations of 2.8 and 10.7 mg/kg and average crustal density of 2.5 g/cm<sup>3</sup> (Rudnick and  
360 Fountain, 1995) the estimated age of filling of the of Boggy Creek field is 32 Ma (Fig 5). Assuming ± 5  
361 % and ± 10 % uncertainty in porosity and <sup>238</sup>U and <sup>232</sup>Th concentrations respectively, the  
362 accumulation age could vary between 22 and 45 Ma (showed in shaded area in Fig 5). The model  
363 only considers <sup>4</sup>He accumulated in-situ and does not account for other <sup>4</sup>He sources in the total  
364 budget which could include: the initial <sup>4</sup>He contents in the gas phase acquired from the source rock,  
365 helium stripped from water during the two stages of methane and CO<sub>2</sub> migration in the reservoir  
366 and any external <sup>4</sup>He flux, caused by heat release associated with regional tectonic events or  
367 volcanism. The model also assumes all radiogenic <sup>4</sup>He produced in the crust is released into the pore  
368 water. Contribution from any of the outlined processes would act to decrease the modelled range,  
369 so the calculated accumulation age range can therefore be taken as a maximum estimate.

370 Methane in Port Campbell traps is associated with the last hydrocarbon generation stage that  
371 commenced during the mid-Paleogene (Duddy, 1997; Boreham et al., 2004), which closely matches  
372 the range of accumulation ages calculated. The <sup>3</sup>He/<sup>4</sup>He ratios observed within the Boggy Creek and  
373 Buttress fields can plausibly be explained by an Argyle-type end-member mixing with methane  
374 containing radiogenic <sup>4</sup>He, confirming the binary mixing with methane trend depicted in Figure 4.



375

376 **Figure 5.  $^3\text{He}/^4\text{He}$  ratio vs time since gas emplacement calculated for the composition of the Boggy Creek-1**  
 377 **sample. To achieve the current  $^3\text{He}/^4\text{He}$  ratio measured in Boggy Creek (1.21  $R_A$ ), Argyle-type  $\text{CO}_2$  (3.65  $R_A$ )**  
 378 **would have to mix with methane that has been emplaced at 32 Ma. Shaded area shows uncertainty.**

379 The same calculation can be applied to the  $\text{CO}_2$  springs. The  $^{238}\text{U}$ - $^{232}\text{Th}$  contents are assumed  
 380 to be the same; the porosity of a fracture-dominated metasedimentary aquifer is estimated to be  
 381 lower ( $10 \pm 5\%$ ). To reduce the initial  $^3\text{He}/^4\text{He}$  ratios of 3.65 to the lowest measured value of 1.23  $R_A$ ,  
 382 it would take 9 Ma years on average and between 4-15 Ma within the uncertainty of the parameters.  
 383 To account for the range of observed  $^3\text{He}/^4\text{He}$  ratios, this scenario requires emplacement of separate  
 384 gas pockets for each individual spring at different times between 9 Ma and present and retention  
 385 within the crust before the onset of the recent migration to the surface.

386 Multiple gas injection events could be associated with discrete episodes of seismic or volcanic  
 387 activity, although the latter is unlikely because the volcanic cones are far fewer than the individual  
 388 mineral springs (>100) (Shugg, 2009), and given the predominately monogenetic eruptive character  
 389 of the NVP extrusives (Boyce, 2013) volcanic activity is unlikely to produce so many different gas  
 390 pulses. Irrespective of the gas emplacement mechanism, the heavily folded and fractured Ordovician  
 391 metasedimentary sequence is unlikely to act as an effective gas trap for millions of years. In-situ  $^4\text{He}$   
 392 accumulation in  $\text{CO}_2$  springs is therefore an unlikely process to account for the observed variation in  
 393  $^3\text{He}/^4\text{He}$  ratios.

#### 394 4.2.2. Radiogenic $^4\text{He}$ stripping from enriched pore-water

395 An alternative model to in-situ generation is modification of magmatic  $^3\text{He}/^4\text{He}$  ratios by  
 396 dilution of mantle He by interaction with radiogenic helium-rich basement fluids during lateral

397 movement of the CO<sub>2</sub>. Stagnant fluids in basement rocks with high U/Th concentrations are enriched  
 398 in radiogenic <sup>4</sup>He well above ASW levels with <sup>3</sup>He/<sup>4</sup>He ratios in the crustal range (0.02 R<sub>A</sub>) (Bottomley  
 399 et al., 1984; Weinlich et al., 1999; Holland et al., 2013; Warr et al., 2018). Isolated stagnant pockets  
 400 of these fluids within the Cambrian – Ordovician basement sequence are a likely source of <sup>4</sup>He for  
 401 the migrating mantle CO<sub>2</sub>. In this case, the process is still governed by the helium production rate in  
 402 the crust (similar to the in-situ <sup>4</sup>He accumulation discussed above), but the controlling factor is  
 403 distance migrated through the basement rather than time.

404 Samples with higher <sup>3</sup>He/<sup>4</sup>He ratios are located geographically closer to each other and the  
 405 Muckleford fault zone. Under the assumption that one of these major fault zones could provide a  
 406 pathway for mantle CO<sub>2</sub> ascent to the surface, we can infer that the spring with the highest  
 407 measured <sup>3</sup>He/<sup>4</sup>He ratio (Argyle, 3.65 R<sub>A</sub>) would be the closest to the main conduit. Figure 6a shows  
 408 the relationship between the <sup>3</sup>He/<sup>4</sup>He ratios and the radial distance of sample location to the Argyle  
 409 spring. Kyneton spring is excluded from this because of its contamination with an atmospheric  
 410 component. The observed <sup>3</sup>He/<sup>4</sup>He ratios consistently decrease with increasing distance from the  
 411 inferred conduit, suggesting mantle CO<sub>2</sub> is being progressively diluted with a crustal component with  
 412 increasing distance migrated through the basement.

413 The mechanism of interaction with these fluids depends on whether CO<sub>2</sub> migrates in the gas phase  
 414 or dissolved in water. In case of the former, the governing factor is differences in solubility as helium  
 415 is strongly partitioned from the fluid to the migrating gas phase. If CO<sub>2</sub> migrates dissolved in water,  
 416 the mixing with the crustal fluids can be described by a mechanical dispersion model (Sano et al.,  
 417 1990). Assuming that mantle fluids are supplied through a single conduit at a constant rate under  
 418 steady-state homogeneous and isotropic conditions under an equal hydrostatic pressure, <sup>3</sup>He/<sup>4</sup>He is  
 419 calculated as a function of the radial distance to the conduit (*r*) following the approach detailed in  
 420 Sano et al. (1990) of deriving the location-specific helium dispersion constant (*α*) by fitting a least  
 421 squares function to the measured <sup>3</sup>He/<sup>4</sup>He and radial distance data points.

$$422 \quad \frac{{}^3\text{He}}{{}^4\text{He}}(r) = \left( \frac{{}^3P r^2 + \alpha {}^3\text{He}_m}{{}^4P r^2 + \alpha {}^4\text{He}_m} \right) \quad (4)$$

423 Where:

424 *r* – radial distance from the main gas conduit

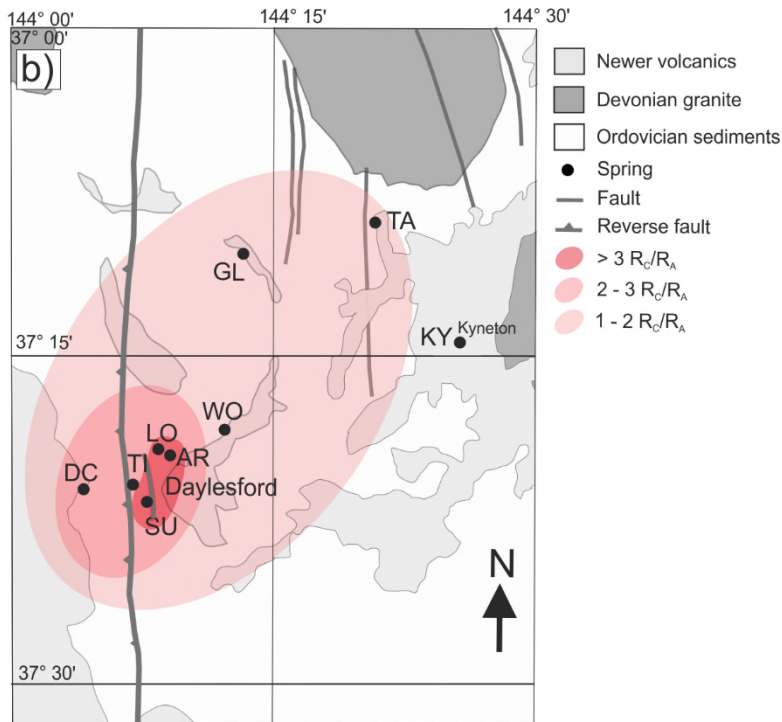
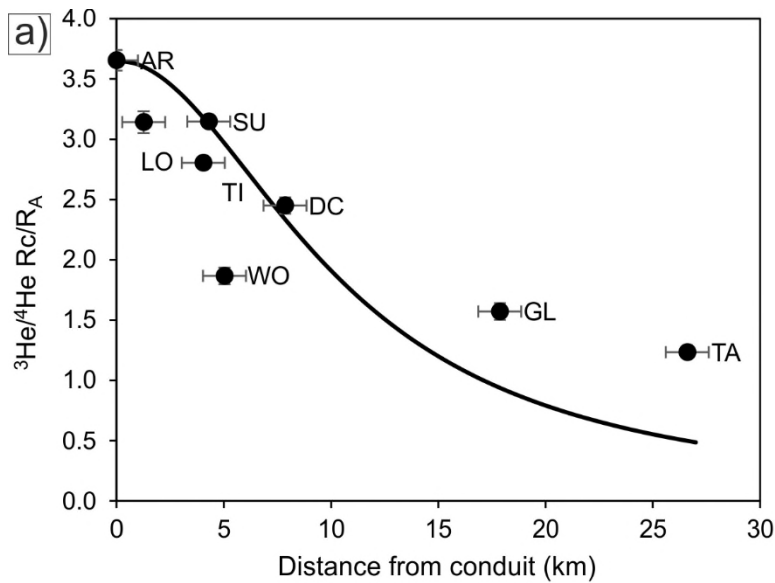
425 *α* – helium dispersion constant, dependent on the pore network geometry

426 *P* – crustal helium production rate in atoms/cm<sup>3</sup>s, calculated under the same crustal density and U,  
 427 Th content assumptions as in the <sup>4</sup>He accumulation model.

428 Similar decreases in  $^3\text{He}/^4\text{He}$  ratios with increasing distance from a central volcanic cone has been  
429 observed in various active volcanoes (Marty and Jambon, 1987; Williams et al., 1987; Sano et al.,  
430 1990; Sakamoto et al., 1992). The calculated hydrodynamic dispersion coefficient (methods in Sano  
431 et al., 1990) is  $0.035 \text{ cm}^2/\text{s}$ , which compares well with the estimates in the original model ( $0.09$  and  
432  $0.055 \text{ cm}^2/\text{s}$ ).

433 The overall average rate of  $^3\text{He}/^4\text{He}$  decrease in 4 volcanic locations reviewed by Sakamoto et al.  
434 (1992) varied between  $0.3$  to  $0.5 R_A/\text{km}$ . The average rate of  $^3\text{He}/^4\text{He}$  decrease in CVH is  $0.1 R_A/\text{km}$ ,  
435 potentially reflecting fluid migration via more efficient fracture networks and conduits in a faulted  
436 sequence relative to the previously investigated volcanic and volcanoclastic sequences. Fractured  
437 aquifers have lower tortuosity relative to porous ones, which results in shorter effective travel  
438 distance for the same total flow path distance (Clennell, 1997) and therefore lower rate of  
439 interaction with radiogenic basement fluids per distance travelled.

440 Springs with the highest  $^3\text{He}/^4\text{He}$  ratios are clustered near the N-S trending Muckleford Fault  
441 and a smaller parallel fault striking along Lake Daylesford (Fig 6b). Previous studies have shown that  
442 clusters of NVP volcanic vents are commonly aligned parallel to nearby basement faults throughout  
443 the province (van Otterloo et al., 2013; Cas et al., 2017). Mantle xenoliths were found in the vicinity  
444 of the faults, suggesting fast mantle upwelling rates through the lithosphere were prevalent during  
445 periods of magmatic activity (van Otterloo et al., 2014). While further work is required to provide  
446 geomechanical and structural geological evidence for current fluid migration along the fault zones in  
447 the CVH, the spatial distribution of  $^3\text{He}/^4\text{He}$  ratios suggests that these basement lineaments  
448 potentially play an important role in the currently active mantle- $\text{CO}_2$  ascent to the surface.



449

450 **Figure 6 a).** Plot of  $^3\text{He}/^4\text{He } R_c/R_A$  values relative to the distance from the Argyle spring (highest  $^3\text{He}/^4\text{He}$   
 451 **ratio), inferred to be closest to the conduit.  $^3\text{He}/^4\text{He}$  ratios decrease with increasing radial distance. The**  
 452 **solid line is  $^3\text{He}/^4\text{He}$  dispersion with distance model calculated based on Sano et al. (1990). b) Geographical**  
 453 **distribution of CO<sub>2</sub> springs. Springs with the highest  $^3\text{He}/^4\text{He}$  ratios are clustered close to N-S trending**  
 454 **basement-scale Muckelford thrust fault and parallel smaller fault near Lake Daylesford. Shaded areas show**  
 455  **$^3\text{He}/^4\text{He}$  ratio ranges which decrease with increasing distance from the Argyle spring. Kyneton spring is**  
 456 **excluded due to atmospheric contamination. Abbreviations of sample names are given in Table 1.**

### 457 4.3. Evaluating models to account for CO<sub>2</sub>/<sup>3</sup>He and δ<sup>13</sup>C(CO<sub>2</sub>) variation

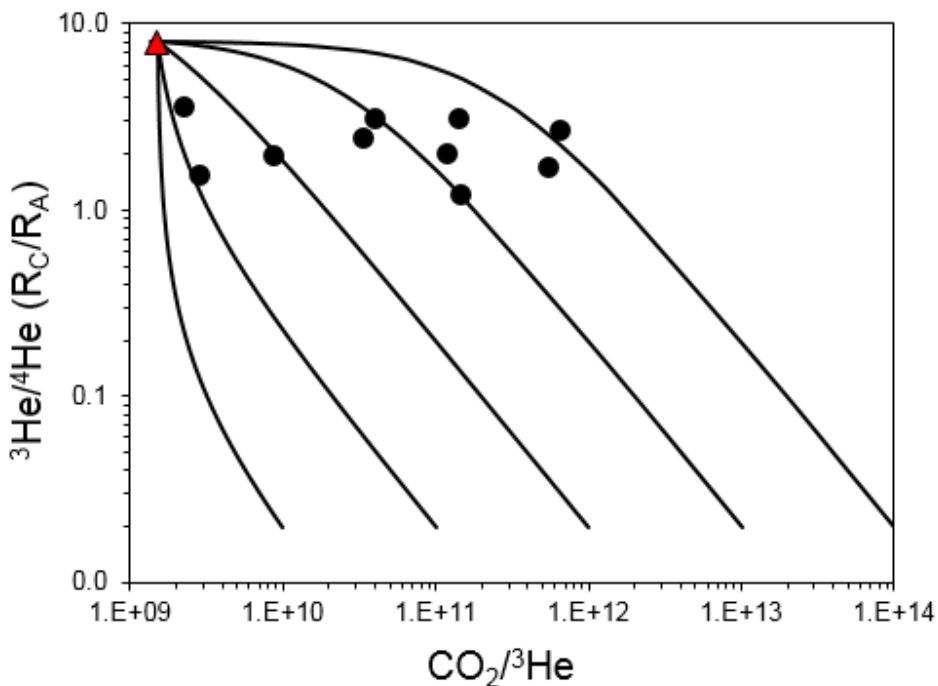
458 The combination of CO<sub>2</sub>, helium and δ<sup>13</sup>C(CO<sub>2</sub>) values is commonly used to identify the  
459 presence of mantle volatiles. This is because CO<sub>2</sub>/<sup>3</sup>He ratios have been well constrained for mantle-  
460 derived melts, fluids and volatiles, with an average MORB value accepted as 1.5 ± 0.5 × 10<sup>9</sup> (Sano and  
461 Marty, 1995; Marty and Tolstikhin, 1998). <sup>3</sup>He is not produced in significant amounts in the crust, so  
462 low <sup>3</sup>He/<sup>4</sup>He ratios and associated CO<sub>2</sub>/<sup>3</sup>He ratios between 10<sup>10</sup> – 10<sup>15</sup> are typically associated with a  
463 crustal CO<sub>2</sub> source (O’Nions and Oxburgh, 1988). The CO<sub>2</sub>/<sup>3</sup>He ratios observed in ten CO<sub>2</sub> samples  
464 from the Victorian mineral springs vary over two orders of magnitude (2.8 × 10<sup>9</sup> to 6.5 × 10<sup>11</sup>),  
465 encompassing the range typical of mantle and crust end-members. A trend in increasing CO<sub>2</sub>/<sup>3</sup>He  
466 ratios is therefore commonly associated with admixture of crustal CO<sub>2</sub> and/or degassing in open  
467 system (e.g. Crossey et al., 2009; Newell et al., 2015; Ruzié et al., 2013), defined by Rayleigh  
468 fractionation. Here, we test both of these possibilities.

469 Crustal end-members can have a wide range of CO<sub>2</sub>/<sup>3</sup>He ratios but a narrow range of <sup>3</sup>He/<sup>4</sup>He  
470 ratios (0.01 – 0.07 R<sub>A</sub>) (Ozima and Podosek, 2002). Figure 7 shows CO<sub>2</sub>/<sup>3</sup>He values plotted against  
471 <sup>3</sup>He/<sup>4</sup>He R<sub>c</sub>/R<sub>A</sub> ratios with binary mixing curves representing mantle (8 R<sub>A</sub>) source and various crustal  
472 components. Significantly, samples with high CO<sub>2</sub>/<sup>3</sup>He ratios do not necessarily show lower <sup>3</sup>He/<sup>4</sup>He  
473 ratios, as would be expected in the case of mixing with <sup>3</sup>He-poor crustal CO<sub>2</sub> source and trend  
474 perpendicular to the calculated mixing lines. To explain the range of measured CO<sub>2</sub>/<sup>3</sup>He ratios,  
475 variable amounts of mixing with a wide range of different crustal reservoirs (CO<sub>2</sub>/<sup>3</sup>He – 10<sup>10</sup> - 10<sup>14</sup>)  
476 would need to be invoked, which is unlikely in the setting where bedrock lithology is uniform across  
477 the area.

478 Crustal CO<sub>2</sub> addition can be further assessed by combining He data with δ<sup>13</sup>C(CO<sub>2</sub>) values  
479 (Sano and Marty, 1995). The range of δ<sup>13</sup>C(CO<sub>2</sub>) values measured in the springs (-9.4 to -6‰) partly  
480 overlap the typical mantle range (-7 to -4‰) (Wycherley et al., 1999). However, increasing CO<sub>2</sub>/<sup>3</sup>He  
481 ratios do not consistently correlate with δ<sup>13</sup>C(CO<sub>2</sub>) change towards carbonate or organic end-  
482 members (Fig. 8). Instead, a vertical trend exists, which would require mixing with an end-member  
483 with constant proportions of both organic and carbonate-sourced CO<sub>2</sub>. To explain the highest  
484 observed CO<sub>2</sub>/<sup>3</sup>He ratios, 99 % of non-mantle (crustal/organic mixture) CO<sub>2</sub> addition is required. Such  
485 significant amounts of crustal CO<sub>2</sub> sourced by dissolution of bedrock minerals would liberate cations  
486 contained in the dissolving minerals and increase the TDS values of the water. Figure 9 shows that  
487 there is no clear positive correlation between the CO<sub>2</sub>/<sup>3</sup>He ratios in the volatiles and TDS values in  
488 their associated waters. Alternatively, CO<sub>2</sub> and helium loss during open system degassing can be  
489 evaluated using Rayleigh fractionation modelling. Figure 8 also shows a calculated open system

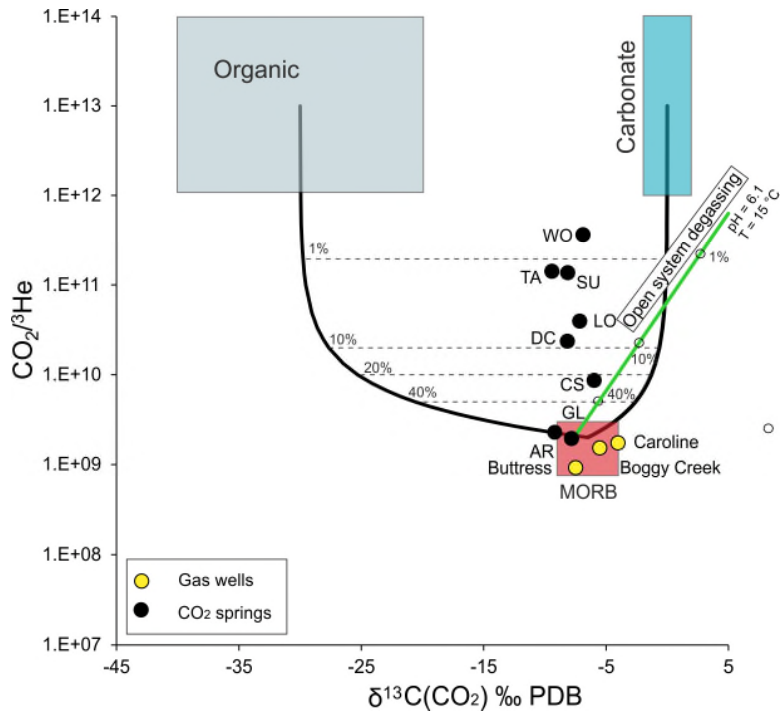
490 Rayleigh fractionation line, assuming average pH of 6.1 and 15 °C temperature. The calculated  
 491 fractionation factor between He/CO<sub>2</sub> is 0.012; the enrichment factor  $\ln 10^3 \alpha \delta^{13}\text{C}(\text{CO}_2)_{\text{aq}}/(\text{CO}_2)_{\text{g}}$  is  
 492 2.2‰. Open system degassing under measured conditions would result in a similar fractionation in  
 493 CO<sub>2</sub>/<sup>3</sup>He ratio but a significantly more extensive than observed fractionation of  $\delta^{13}\text{C}(\text{CO}_2)$  values. We  
 494 therefore conclude that degassing under open system conditions is not supported by the data.

495 Previous geochemical modelling work showed that CO<sub>2</sub> does not cause significant amounts of  
 496 bedrock mineral dissolution in the Ordovician aquifer (Karolytè et al., 2017) and there is no  
 497 geological evidence for addition of large amounts of crustal CO<sub>2</sub> from other sources (e.g. carbonate  
 498 metamorphism). The possibility of significant amounts of organic CO<sub>2</sub> addition is also ruled out,  
 499 because the observed trend on Figure 8 cannot be explained by addition of organic CO<sub>2</sub> in the  
 500 absence of the crustal component. Based on the combined evidence from  $\delta^{13}\text{C}(\text{CO}_2)$ -He, CO<sub>2</sub>  
 501 abundance and TDS contents of the mineral waters, we conclude that there is no significant crustal  
 502 CO<sub>2</sub> addition to the mantle volatiles sampled at the CVH and Clifton Springs. CO<sub>2</sub> loss during  
 503 degassing under open system conditions is also not supported by the data.



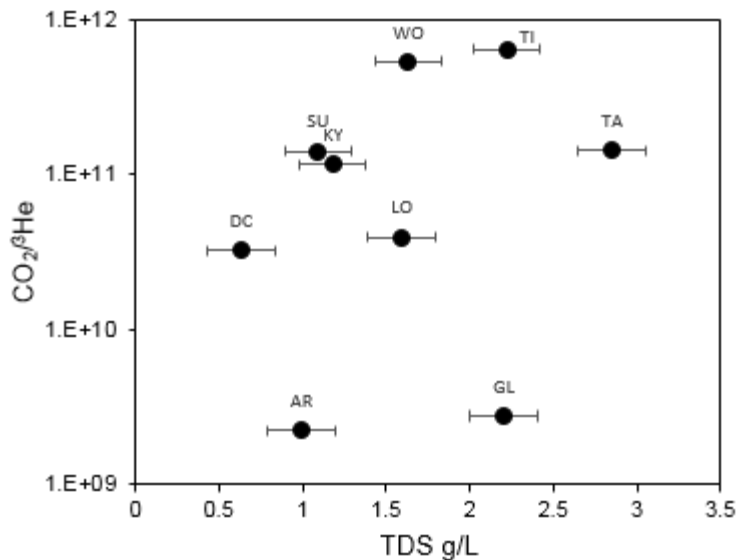
504  
 505 **Figure 7. Binary mixing plot between MORB (red triangle) (<sup>3</sup>He/<sup>4</sup>He 8 R<sub>A</sub>, CO<sub>2</sub>/<sup>3</sup>He 1.5 x 10<sup>9</sup>) and various**  
 506 **crustal end-members (CO<sub>2</sub>/<sup>3</sup>He 10<sup>10</sup>-10<sup>14</sup>). The springs form a near-horizontal trendline and do not follow**  
 507 **any of the mixing lines, suggesting that mixing does not control the variation in CO<sub>2</sub>/<sup>3</sup>He values. All error**  
 508 **bars are smaller than the printed symbols.**





509

510 **Figure 8.  $\text{CO}_2/{}^3\text{He}$  ratios vs  $\delta^{13}\text{C}(\text{CO}_2)$  values for gas samples in relation to mixing between the mantle,**  
 511 **carbonate and organic  $\text{CO}_2$  end-members based on Sano and Marty (1995). Caroline, Boggy Creek and**  
 512 **Buttruss well gases fall within the mantle range. Spring samples do not show a coherent trend towards**  
 513 **either an organic or carbonate  $\text{CO}_2$  end member. The observed trend would require > 99% contribution of a**  
 514 **component with constant proportions of both organic and carbonate-sourced  $\text{CO}_2$ . Green line shows**  
 515 **Rayleigh fractionation during degassing under average measured pH and temperature, open circles indicate**  
 516 **percentage of gas left. The data do not fall on either the mixing or open system degassing curves (discussed**  
 517 **in text). Abbreviations of sample names are given in Table 1.**



518

519 **Figure 9. CO<sub>2</sub>/<sup>3</sup>He vs TDS measured in water, sampled via hand pumps from tube bores. CO<sub>2</sub>/<sup>3</sup>He values are**  
 520 **not correlated with TDS. A positive correlation would be expected if crustal CO<sub>2</sub> were added as a result of**  
 521 **bedrock mineral dissolution.**

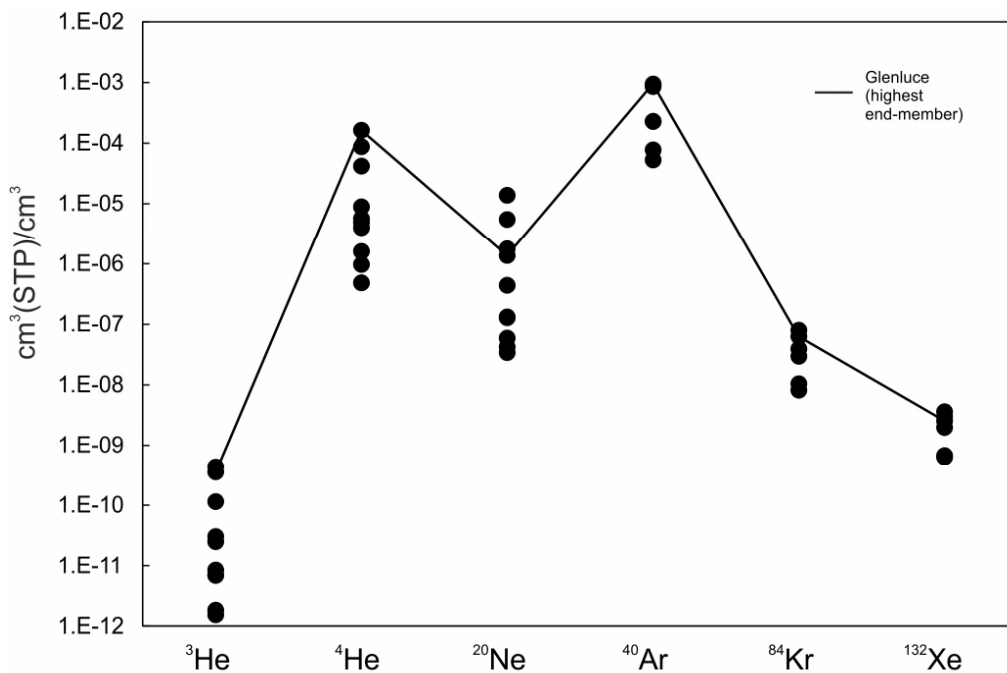
522 Alternatively to mixing with different CO<sub>2</sub> sources, the variability of δ<sup>13</sup>C(CO<sub>2</sub>) values (-9.4 to -  
 523 6‰) can be explained by degassing in separate individual systems under a range of different pH and  
 524 temperature conditions. Equilibrium fractionation between δ<sup>13</sup>C(CO<sub>2</sub>) in aqueous and gaseous  
 525 phases is controlled by the temperature and the relative amounts of HCO<sub>3</sub><sup>-</sup> and H<sub>2</sub>CO<sub>3</sub>, which are pH-  
 526 dependent. If H<sub>2</sub>CO<sub>3</sub> is the dominant dissolved inorganic carbon (DIC) species, degassing CO<sub>2</sub> is  
 527 slightly enriched in <sup>13</sup>C. Conversely, when HCO<sub>3</sub><sup>-</sup> dominates the system, degassing CO<sub>2</sub> is relatively  
 528 depleted in <sup>13</sup>C (Deines et al., 1974). The pH values measured in mineral water bores range from 5.5  
 529 to 6.1 and temperatures are 15 – 21 °C. In this particular range of conditions, the ratio of HCO<sub>3</sub><sup>-</sup> to  
 530 H<sub>2</sub>CO<sub>3</sub> in DIC varies significantly. The resulting calculated equilibrium enrichment factors between  
 531 DIC and gaseous CO<sub>2</sub> range from -3.4 to -0.43‰. Degassing under different DIC speciation conditions  
 532 therefore can fully account for the observed 3.4‰ variability in δ<sup>13</sup>C(CO<sub>2</sub>) values of the spring gases.

533 The trends observed in our data are not unique to this study. CO<sub>2</sub>/<sup>3</sup>He ratios ranging between  
 534 10<sup>9</sup> to 10<sup>14</sup> combined with δ<sup>13</sup>C(CO<sub>2</sub>) values without an obvious trend towards organic or carbonate  
 535 end-member is a common observation, commonly interpreted as a result of simple mantle and  
 536 crustal end-member mixing (Aka et al., 2001; Crossey et al., 2009; Mao et al., 2009). Other workers  
 537 recognised that simple mixing is not a conclusive interpretation (Italiano et al., 2014) and suggested  
 538 contribution of a solubility fractionation process (Matthews et al., 1987; Hilton, 2009; Newell et al.,  
 539 2015). Where open system Rayleigh fractionation is proposed, it is commonly not conclusively  
 540 supported by evidence from δ<sup>13</sup>C(CO<sub>2</sub>) values (Ruzié et al., 2013; Bräuer et al., 2016). In the following

541 section, we explore how this trend can alternatively be explained by fractionation during a two-step  
 542 process of dissolution and degassing.

#### 543 4.4 Noble gas abundance modification by solubility in water

544 The variation observed in <sup>3</sup>He concentrations in the mineral spring samples is also replicated in <sup>4</sup>He  
 545 and other noble gases. Figure 10 shows the distribution of noble gas concentrations in all studied  
 546 springs. Importantly, the variance in observed gas concentrations decreases with element mass (Fig.  
 547 10), indicating a solubility-controlled process. If mantle CO<sub>2</sub> is transported to the surface in solution,  
 548 this process can be modelled as dissolution and subsequent degassing.



549 **Figure 10. Noble gas concentrations of CO<sub>2</sub> spring samples in cm<sup>3</sup> (STP)/cm<sup>3</sup>. The variation in concentrations**  
 550 **decreases with increasing molecular mass. Solid black line shows the concentrations measured in Glenluce**  
 551 **spring, which has the highest helium concentrations and least fractionated CO<sub>2</sub>/<sup>3</sup>He ratios.**  
 552

554 During the equilibration between gas and water, noble gases are partitioned between the phases  
 555 according to their solubility coefficient, as defined by Henry's Law:

$$556 C_{iw} = \frac{C_{ig}}{K_i} \quad (5)$$

557 Where C is concentration, subscripts g and w denote gas and water phases and K<sub>i</sub> is dimensionless  
 558 Henry's constant for noble gas i. K<sub>i</sub> is temperature, pressure and salinity dependent (Kipfer et al.,  
 559 2002). The final concentrations in both phases depend on the volumetric gas/water ratio. The  
 560 equilibrium concentrations in the water ( $C_{iw}^{eq}$ ) are expressed as (Zartman et al., 1961):

561  $C_{iw}^{eq} = C_{it} \times F_w$  (6)

562  $F_w = \frac{C_{iw}V_w}{C_{iw}V_w + C_{ig}V_g}$  (7)

563 Where V is volume,  $C_{it}$  is the total noble gas budget, and  $F_w$  is the fraction of noble gases in the  
 564 water. Combining equations 5-7,  $C_{iw}^{eq}$  is:

565  $C_{iw}^{eq} = C_t \times (1 + \frac{V_g}{V_w} K_i)^{-1}$  (8)

566 After the equilibration step, the water and the gas source separate and ascend to the surface  
 567 independently. The gases collected at the surface of stream beds are assumed to have been  
 568 transported in solution. During degassing at the surface, the noble gases are partitioned between  
 569 the phases again. The final measured gas concentrations are:

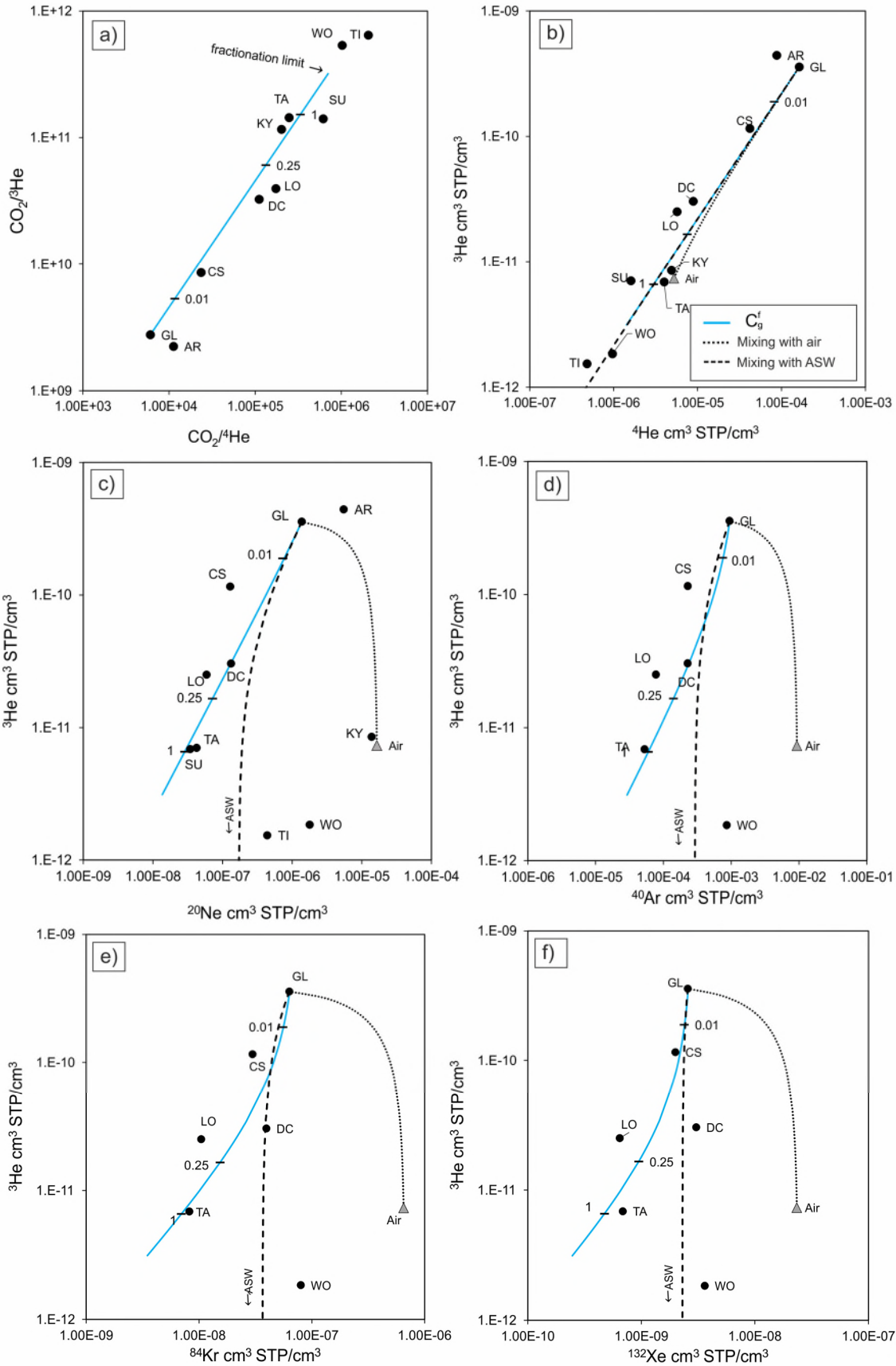
570  $C_{ig}^f = C_{iw}^{eq} \times (1 + (\frac{V_g}{V_w})^{-1} \frac{1}{K_i})^{-1}$  (9)

571 For the purpose of investigating a shallow degassing process, equilibration with fresh water at  
 572 atmospheric pressure and 20 °C temperature is assumed. Henry's constants and activity coefficients  
 573 for water conditions were calculated from empirical equations from Crovetto et al. (1982) for Ne, Ar,  
 574 Kr and Xe and Smith (1985) for He, following the methodology in Ballentine and Burnard (2002).  
 575 Henry's constant for CO<sub>2</sub> is calculated using empirical equations from Crovetto (1991). Assuming the  
 576 density of fresh water (0.996 cm<sup>3</sup>/g) (Weast et al., 1988), concentrations in ASW are converted from  
 577 cm<sup>3</sup>STP/g<sub>H<sub>2</sub>O</sub> to cm<sup>3</sup>STP/cm<sup>3</sup> for Figure 11.

578 The highest helium concentrations and lowest CO<sub>2</sub>/<sup>3</sup>He ratio were measured in the Glenluce spring.  
 579 We therefore assume that Glenluce is the least solubility fractionated end-member. For the purpose  
 580 of the model, we make a simplifying assumption that the Glenluce sample represents the total  
 581 amount of CO<sub>2</sub> and noble gases from both the mantle and ASW sources ( $C_t$ ). This end-member  
 582 equilibrates with a volume of water which, in theory, is noble gas free. When  $\frac{V_g}{V_w} \rightarrow 0$ ,  $F_w \rightarrow 1$ , all  
 583 gases are dissolved in water. All gas contents are transferred into the water phase  $C_{iw}^{eq}$  and the ratios  
 584 are equal to the initial ones. When  $\frac{V_g}{V_w} \rightarrow \infty$  and  $F_w \rightarrow 0$ , only a small fraction of noble gas contents  
 585 are dissolved in water. In this case, the ratios are the most fractionated and the concentrations in  
 586 water are low. After the equilibration, the water separates from the gas source, migrates to the  
 587 surface and degasses. We make a simplifying assumption that the water degasses entirely,  $\frac{V_g}{V_w} \rightarrow \infty$ ,  
 588 all dissolved gases are transferred into the gas phase and therefore the final measured  $C_{ig}^f \rightarrow C_{iw}^{eq}$ .

589 Figure 11 shows CO<sub>2</sub>/He ratios, <sup>3</sup>He concentrations relative to <sup>4</sup>He, <sup>20</sup>Ne, <sup>40</sup>Ar, <sup>84</sup>Kr and <sup>132</sup>Xe and the  
590 calculated solubility curves  $C_{ig}^f$ . The data points fall on the modelled line and is clearly  
591 distinguishable from mixing with ASW, which is more enriched in all atmospheric noble gases. Air  
592 and ASW components are potentially introduced by inclusion of small amounts of air and water into  
593 the copper tube during sampling and are the most significant in Kyneton, Tipperary and Woolnoughs  
594 samples. Tipperary and Woolnoughs springs include a combination of ASW and air components,  
595 which is obvious in different element pair plots (Fig. 11 c,d,e,f) and less apparent in <sup>3</sup>He vs <sup>4</sup>He (Fig.  
596 11b) because air and ASW have similar <sup>3</sup>He/<sup>4</sup>He ratios. Figure 11b also clearly shows that the original  
597 concentrations in Kyneton spring have been overprinted by admixture of air, most likely during  
598 sample collection and clearly identified in the <sup>4</sup>He/<sup>20</sup>Ne ratios. The ASW component is more evident  
599 in the heavier atmospheric noble gases in the Deep Creek sample (Fig. 11 ,d,e,f).

600 With the exceptions discussed above, all other samples plot close to the modelled solubility  
601 fractionation line. The maximum extent of fractionation between CO<sub>2</sub> and He is limited by the ratio  
602 of Henry's constants  $K_{CO_2}/K_{He}$  (Fig. 11a). The calculated  $\frac{V_g}{V_w}$  ratios and progressive loss of noble gas  
603 concentrations with decreasing F are consistent across all noble gas elemental pairs. When  $\frac{V_g}{V_w}$  is  
604 unity, 47% of the total CO<sub>2</sub> is dissolved but only 1% of helium. The resulting CO<sub>2</sub>/<sup>3</sup>He ratio is 1.4 x  
605 10<sup>11</sup>, which is the highest in the sample group, excluding the previously discussed samples which are  
606 contaminated with air. This means that dissolution in water under equal gas/water ratios explains  
607 the maximum observed fractionation of CO<sub>2</sub>/<sup>3</sup>He values. According to the model, the minimum  $\frac{V_g}{V_w}$   
608 ratio required to dissolve the entire sample without fractionating the CO<sub>2</sub>/<sup>3</sup>He is 0.0005, or 2000  
609 times more water than gas.



610  
611  
612

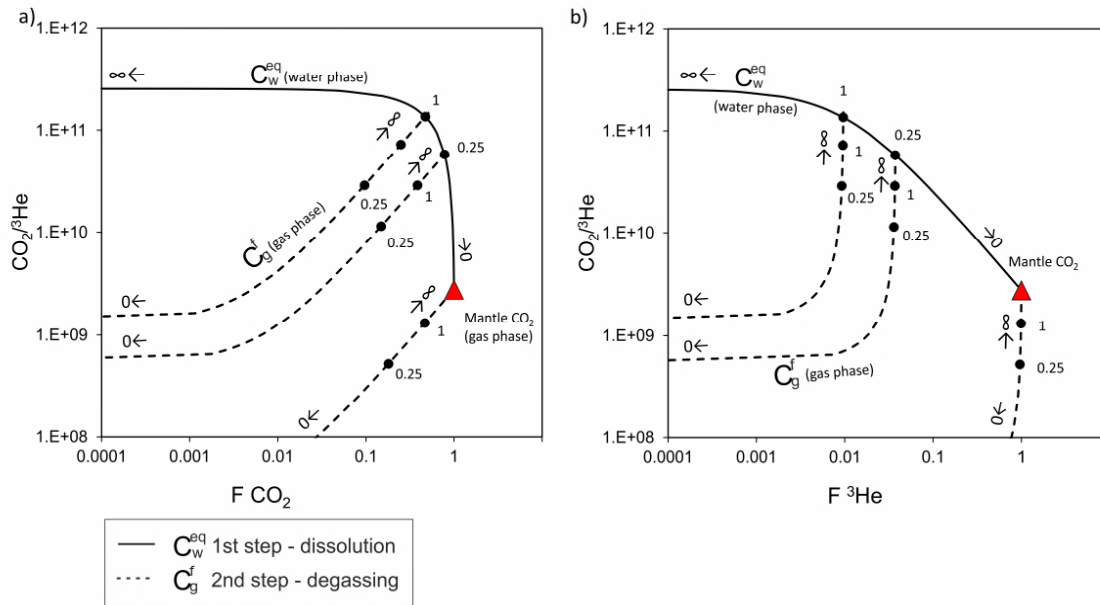
Figure 11.  $\text{CO}_2/\text{He}$  ratios (a) and  $^3\text{He}$  concentrations relative to  $^4\text{He}$  (b),  $^{20}\text{Ne}$  (c),  $^{40}\text{Ar}$  (d),  $^{84}\text{Kr}$  (e) and  $^{132}\text{Xe}$  (f) in  $\text{cm}^3(\text{STP})/\text{cm}^3$ . The solid blue line shows the concentrations in the gas phase after a two-step dissolution

613 and degassing. First, water equilibrates with gas under different gas/water ratios. Second, the water of that  
614 composition degasses entirely. Tick marks show gas/water ratios during the dissolution stage. Dashed lines  
615 show mixing with ASW at 20 °C; dotted line shows mixing with air. Some deviations from the modelled line  
616 occur due to mixing with ASW and/or air. a) The extent of CO<sub>2</sub>/He fractionation during dissolution is limited  
617 by  $K_{CO_2}/K_{He}$ . All samples fall within this range except for TI and WO. c) shows that this is because TI and WO  
618 have a contribution between ASW and air components, plotting between these end-members. This is  
619 consistently replicated for Woolnoughs spring in c) d) and e). Ar, Kr and Xe concentrations of CS, DC, LO and  
620 TA springs are within the limits of mixing with ASW and calculated model line. Abbreviations of sample  
621 names are given in Table 1.

622

623 The model results are not a strict interpretation of the geological system, but rather an indication of  
624 how the water controls the noble gas budget. The samples with high noble gas concentrations and  
625 mantle CO<sub>2</sub>/<sup>3</sup>He ratios might alternatively be interpreted to represent the residual gas cap migrating  
626 the gas phase after the equilibration with water or having had minimal interaction with the water.  
627 However, in cases where gas migrates dissolved in water and degasses at the surface, equilibration  
628 in equal volumes of gas and water is needed to fractionate the CO<sub>2</sub>/<sup>3</sup>He ratios by two orders of  
629 magnitude. This is a significant consideration for the use of CO<sub>2</sub>/<sup>3</sup>He ratios in interpretation of gas  
630 provenance in gases equilibrating with water.

631 Figure 12 shows a theoretical fractionation model of mantle-derived CO<sub>2</sub> under the same ambient  
632 atmospheric conditions as the previous model. A sample with the starting concentrations of [CO<sub>2</sub>] =  
633 0.99 and [<sup>3</sup>He] = 1.2 x 10<sup>-12</sup> cm<sup>3</sup>STP/cm<sup>3</sup> is dissolved in water under different gas/water ratios. The  
634 figure shows how the decreasing fraction of moles relative to the starting value, transferred to the  
635 water and gas phases during the two-stage process, translates to CO<sub>2</sub>/<sup>3</sup>He ratios. When the  
636 gas/water ratio is low during the dissolution step, all gasses are dissolved into the water phase and  
637 the ratio is unchanged. As the gas/water ratio decreases, overall less gas is transferred into the  
638 water phase, but the water becomes more enriched in CO<sub>2</sub> relative to helium. The second step  
639 considers degassing after the equilibration, when the remaining non-dissolved gas is removed from  
640 the system and the water degasses under three scenarios ( $\frac{V_g}{V_w} \rightarrow 0, 0.25$  and 1). This effectively shows  
641 that in a multi-step dissolution and degassing process, the CO<sub>2</sub>/<sup>3</sup>He ratio is entirely dependent on the  
642 gas/water ratios and the extent of fractionation is limited by the ratio of Henry's constants  $K_{CO_2}/K_{He}$ .  
643 In practice, the process is relevant to the point where the gas concentrations are above those in  
644 ASW and the signal is not entirely diluted. Where CO<sub>2</sub> is the main carrier gas, this effect may not be  
645 intuitively obvious, because the measured CO<sub>2</sub> concentrations are always > 99 % and the observed  
646 variation is the <sup>3</sup>He concentrations.



647

648 **Figure 12. Theoretical model of two step dissolution and degassing of mantle  $\text{CO}_2$  and the effect on the**  
 649  **$\text{CO}_2/{}^3\text{He}$  ratio.  $F$  is the fraction of moles in the modelled phase relative to the starting value. Symbols with**  
 650 **arrows indicate  $\frac{V_g}{V_w}$  ratios approaching infinity and zero, black dots mark specific calculated ratios. The solid**  
 651 **black line shows the water phase during dissolution stage (step 1). The dashed lines show the resulting gas**  
 652 **phase after degassing of the water phase under three different scenarios ( $\frac{V_g}{V_w} \rightarrow 0, 0.25, 1$ ) (step 2). The**  
 653 **maximum fractionation of  $\text{CO}_2/{}^3\text{He}$  is limited by the relative ratio of  $K_{\text{CO}_2}/K_{\text{He}}$ .**

654

#### 655 4.4.1. Summary

656 The geological interpretation of the proposed solubility fractionation model requires two stages of  
 657 phase separation - dissolution followed by degassing. Mantle  $\text{CO}_2$  equilibrates with individual  
 658 aquifers under different gas/water ratios. Following this,  $\text{CO}_2$ -saturated water and the remaining gas  
 659 separate and ascend independently, driven by the differences in buoyancy force. Continuous  
 660 seepage of dry  $\text{CO}_2$  (up to 6000 ppm) has been identified in the localised fractures of the Ordovician  
 661 sandstone outcropping near the Tipperary spring (Roberts et al., 2019), confirming the decoupled  
 662  $\text{CO}_2$  and water migration. Water migrates to the surface through individual conduits, forming  
 663 individual mineral water bodies and eventually springs. This model is consistent with the  $\delta^{13}\text{C}(\text{CO}_2)$   
 664 data, explained by degassing under measured temperature and pH conditions with each spring  
 665 acting as a separate system. This appears to be a plausible interpretation of the CVH mineral springs,  
 666 which show high variability in dissolved carbon and cation contents, indicating restricted individual  
 667 aquifers for separate springs (Cartwright et al., 2002; Weaver et al., 2006). Mineral water degasses  
 668 at the surface and all noble gases and  $\text{CO}_2$  are assumed to be stripped from the water phase. The



669 final measured noble gas budgets are strongly controlled by the initial stage of equilibrating with  
670 water.

#### 671 4.5 Model summary and application to CO<sub>2</sub> tracing

672 This case study of south-east Australian CO<sub>2</sub> gas reservoirs and natural springs provides a framework  
673 for investigating genetic link between CO<sub>2</sub> stored in reservoirs and migrating into shallow aquifers.

674 Our findings suggest that the combined helium, CO<sub>2</sub> abundance and  $\delta^{13}\text{C}(\text{CO}_2)$  system allows to  
675 distinguish between key processes that modify the initial geochemical composition: admixture of  
676 crustal or organic sourced CO<sub>2</sub>, mixing with non-CO<sub>2</sub> crustal gases and fractionation between water  
677 and gas phases in either open or closed system. Helium isotopic signature is a particular strength for  
678 source identification in CO<sub>2</sub> spring samples because it can be corrected for atmospheric component.  
679 In contrast, neon and argon isotope ratios are likely to be close to the values of air.

680 A useful way to think about the addition of radiogenic <sup>4</sup>He by addition of non-CO<sub>2</sub> radiogenic  
681 component is to model it as a function of either time or distance. The <sup>4</sup>He dating approach  
682 presented here allows constraint of the residence time needed to accumulate <sup>4</sup>He and use this to  
683 discriminate between alternative interpretations based on their feasibility in the geological context.  
684 While a more comprehensive modelling technique might be needed if an accurate age is the  
685 objective of the study (Zhou and Ballentine, 2006; Liu et al., 2016), this method confirmed in-situ <sup>4</sup>He  
686 accumulation as a viable process in the studied well gases but not in CO<sub>2</sub> springs. The spatial  
687 distribution of <sup>3</sup>He/<sup>4</sup>He ratios in the springs indicated that the distance from the main conduit is a  
688 more important factor in CO<sub>2</sub> springs. This is controlled by the interaction with <sup>4</sup>He-enriched  
689 stagnant basement fluids and can be modelled as fluid dispersion or a solubility process, depending  
690 if CO<sub>2</sub> is assumed to migrate dissolved in water or in a gas phase. In case of the former, our data are  
691 in good agreement with similar observations in volcanic settings (Sano et al., 1990). The latter is also  
692 viable and would produce a similar pattern.

693 Radiogenic <sup>4</sup>He can also be added by mixing with a crustal CO<sub>2</sub> source. In this case, decreasing  
694 <sup>3</sup>He/<sup>4</sup>He ratios should correlate with an increase in CO<sub>2</sub>/<sup>3</sup>He and either a negative or positive shift in  
695  $\delta^{13}\text{C}(\text{CO}_2)$  values, following a trajectory of mixing lines. Alternatively, it is possible that <sup>4</sup>He addition is  
696 decoupled from a secondary phase separation process controlling  $\delta^{13}\text{C}(\text{CO}_2)$  values and CO<sub>2</sub>/<sup>3</sup>He  
697 ratios. In this case, no clear correlation between and CO<sub>2</sub>/<sup>3</sup>He and <sup>3</sup>He/<sup>4</sup>He is expected. If the system  
698 is characterised by progressive gas loss in an open system, generally a significant progressive  
699 enrichment of  $\delta^{13}\text{C}(\text{CO}_2)$  values is expected in non-geothermal temperatures.

700 Alternatively, the sample suite may effectively represent a series of individual systems, where water  
701 and gas equilibrate under different gas/water ratios. In this case, no particular trend is anticipated.  
702 The variation of  $\delta^{13}\text{C}(\text{CO}_2)$  values can instead be controlled by the phase separation at different pH  
703 and temperature conditions. Temperature and pH readings of waters should always be taken to  
704 account for this effect. All noble and major gas concentrations and their relative ratios, including  
705  $\text{CO}_2/{}^3\text{He}$  are modified by dissolution in water and/or degassing, while elemental ratios are not  
706 expected to change. This can be tested by modelling fractionation under different gas/water ratios,  
707 which should be consistent across all element pairs. Importantly, we show how solubility models can  
708 be tested by incorporating Ne, Ar, Kr and Xe concentration data, which are often not interpreted in  
709 natural spring studies because of the air-like isotopic ratios. While  $\text{CO}_2/{}^3\text{He}$  is expected to be easily  
710 modified,  ${}^3\text{He}/{}^4\text{He}$  ratio is not altered by phase partitioning and is a reliable indicator of gas  
711 provenance.

712

## 713 5. Conclusions

714  ${}^3\text{He}/{}^4\text{He}$  and  $\text{CO}_2/{}^3\text{He}$  ratios in well gas and  $\text{CO}_2$  spring samples in the Otway Basin and the  
715 Central Victorian Highlands show unambiguous evidence for a predominantly mantle origin for the  
716  $\text{CO}_2$  stored in the gas fields and actively migrating to the surface at the springs. The main processes  
717 modifying noble gas geochemical signatures are crustal  ${}^4\text{He}$  addition and noble gas elemental  
718 fractionation between the water and gas phases.

719  ${}^3\text{He}/{}^4\text{He}$  ratios in well gases vary due to mixing with methane, which has crustal helium  
720 contents directly dependent on gas residence time in the reservoir. The  ${}^3\text{He}/{}^4\text{He}$  ratio variation in  
721  $\text{CO}_2$  springs is controlled by interaction with  ${}^4\text{He}$ -enriched basement pore fluids and is directly  
722 dependent on the radial distance to the gas supply conduit. The observed decline in  ${}^3\text{He}/{}^4\text{He}$  ratios  
723 with distance suggests that  $\text{CO}_2$  is supplied from a single conduit in the area around Argyle spring.  
724  ${}^3\text{He}/{}^4\text{He}$  ratios are the highest in samples clustered near the Muckleford Fault and smaller parallel  
725 faults in its vicinity, suggesting that one of these basement lineaments could be acting as a pathway  
726 for mantle  $\text{CO}_2$  to reach the shallow subsurface.

727 The variability of noble gas abundance patterns observed in the  $\text{CO}_2$  springs can be explained by  
728 solubility fractionation during equilibration with groundwater. If gas is dissolved in water,  
729 transported and exsolved at the surface, a two-step dissolution and degassing process can be  
730 considered. If gases ascend to the surface dissolved in water, original  $\text{CO}_2/{}^3\text{He}$  ratios are unlikely to  
731 be preserved. In CVH springs,  $\text{CO}_2/{}^3\text{He}$  ratios in the range of  $10^{11} - 10^{12}$  correlate with decreasing

732 concentrations of all noble gases and can be explained by variation of gas/water ratios during  
733 dissolution in water. Gas/water ratios up to 1 during the dissolution stage can explain the maximum  
734 observed fractionation in CO<sub>2</sub>/<sup>3</sup>He ratios. The δ<sup>13</sup>C(CO<sub>2</sub>) values are controlled by dissolution and  
735 degassing at pH range of 5.8 - 6.3. This internally consistent model explains the abundance and  
736 isotopic signature in He, Ne, Ar, Kr, Xe and δ<sup>13</sup>C(CO<sub>2</sub>).

737 Taking these processes into account, noble gas compositions observed in well gases in Port  
738 Campbell, Mount Gambier, as well as CO<sub>2</sub> springs in CVH and Clifton Springs are traced back to a  
739 single end member of <sup>3</sup>He/<sup>4</sup>He of 3.07 - 3.65 R<sub>A</sub>, proving a common source. This implies a uniform  
740 regional gas composition in the Otway basin and CVH.

741 Importantly, we present evidence that <sup>3</sup>He loss resulting in high CO<sub>2</sub>/<sup>3</sup>He ratios, commonly  
742 associated with crustal CO<sub>2</sub> addition, can be explained without the need to invoke mixing with  
743 crustal CO<sub>2</sub>, which is especially important in the absence of a clear mixing trend in δ<sup>13</sup>C(CO<sub>2</sub>) values.  
744 Hence, CO<sub>2</sub>/<sup>3</sup>He values should be compared to the concentrations of other noble gases and used  
745 with caution when assessing the origin of CO<sub>2</sub> degassing at surface springs.

746 The techniques outlined in this paper can be used to identify the origin of CO<sub>2</sub> seeps at the  
747 surface and their connectivity to reservoir gases. Hence, they can be applied to CO<sub>2</sub> sequestration or  
748 other industrial fugitive gas monitoring settings, such as surrounding shale gas operations. Helium-  
749 CO<sub>2</sub> abundance relationship can be used to determine the gas connectivity as long as the industrial  
750 gas has a different initial He isotope ratio to the ASW end-member. The genetic link between  
751 separate CO<sub>2</sub> seeps can be tested by applying solubility fractionation modelling to account for  
752 changes in noble gas concentrations caused by interaction with water. Noble gases are particularly  
753 sensitive tracers to small-scale gas migration and should be considered for surface monitoring of any  
754 industrial site where emission of fugitive gas is possible.

## 755 Acknowledgments

756 This work was supported by an EPSRC PhD studentship in partnership with CO2CRC and  
757 Badley Geoscience Ltd. G. Johnson and S. Gilfillan were partially supported by both UKCCSRC and  
758 Scottish Carbon Capture and Storage (SCCS), S. Serno was funded by the UK Carbon Capture and  
759 Storage Research Centre (UKCCSRC) Call 2 grant. S. Flude was supported by by EPSRC grant  
760 #EP/K036033/1. We thank the field operators – BOC, Air Liquide and CO2CRC for permission to  
761 sample the gas reservoirs. Craig Vivian and Peter Dumsey are thanked for support while sampling in  
762 the field. We thank Terry Donnelly and Marta Zurakowska at SUERC for assistance in obtaining stable

763 isotope and noble gas measurements of gas samples. Ian Cartwright is thanked for providing  
764 background data on the Daylesford springs.

765

## 766           References

- 767    Aeschbach-Hertig W., El-Gamal H., Wieser M. and Palcsu L. (2008) Modeling excess air and degassing  
768           in groundwater by equilibrium partitioning with a gas phase. *Water Resour. Res.* **44**, 1–12.
- 769    Aka F. T., Kusakabe M., Nagao K. and Tanyileke G. (2001) Noble gas isotopic compositions and  
770           water/gas chemistry of soda springs from the islands of Bioko, São Tomé and Annobon, along  
771           with Cameroon Volcanic Line, West Africa. *Appl. Geochemistry* **16**, 323–338.
- 772    Akbari V. (1992) *Boggy Creek No.1 Well Completion Report.*, Available at: [http://geoscience-web.s3-  
773           website-ap-southeast-2.amazonaws.com/well/boggycreek1.htm](http://geoscience-web.s3-website-ap-southeast-2.amazonaws.com/well/boggycreek1.htm).
- 774    Baines S. J. and Worden R. H. (2004) The long term fate of CO<sub>2</sub> in the subsurface: natural analogues  
775           for CO<sub>2</sub> storage. In *Geological Storage of Carbon Dioxide* (ed. R. H. Baines, S.J., Worden).  
776           Geological Society, London. pp. 59–85.
- 777    Ballentine C. J. and Burnard P. G. (2002) Production, Release and Transport of Noble Gases in the  
778           Continental Crust. *Rev. Mineral. Geochemistry* **47**, 481–538.
- 779    Ballentine C. J. and O’Nions R. K. (1994) The use of natural He, Ne and Ar isotopes to study  
780           hydrocarbon-related fluid provenance, migration and mass balance in sedimentary basins.  
781           *Geol. Soc. London, Spec. Publ.* **78**, 347–361.
- 782    Ballentine C. J., O’Nions R. K. and Coleman M. L. (1996) A Magnus opus: Helium, neon, and argon  
783           isotopes in a North Sea oilfield. *Geochim. Cosmochim. Acta* **60**, 831–848.
- 784    Barry P. H., Lawson M., Meurer W. P., Warr O., Mabry J. C., Byrne D. J. and Ballentine C. J. (2016)  
785           Noble gases solubility models of hydrocarbon charge mechanism in the Sleipner Vest gas field.  
786           *Geochim. Cosmochim. Acta* **194**, 291–309.
- 787    Bernecker T. and Moore D. H. H. (2003) Linking basement and basin fill: implications for hydrocarbon  
788           prospectivity in the Otway Basin Region. *APPEA J.* **43**, 39–58.
- 789    Boreham C. J., Hope J. M., Jackson P., Davenport R., Earl K. L., Edwards D. S., Logan G. A. and Krassay  
790           A. A. (2004) Gas – oil – source correlations in the Otway Basin, southern Australia. In *Petroleum  
791           Exploration Society of Australia (PESA)*. pp. 19–22.
- 792    Boreham C., Underschultz J., Stalker L., Kirste D., Freifeld B., Jenkins C. and Ennis-King J. (2011)  
793           Monitoring of CO<sub>2</sub> storage in a depleted natural gas reservoir: Gas geochemistry from the  
794           CO<sub>2</sub>CRC Otway Project, Australia. *Int. J. Greenh. Gas Control* **5**, 1039–1054.

- 795 Bosch A. and Mazor E. (1988) Natural gas association with water and oil as depicted by atmospheric  
796 noble gases: case studies from the southeastern Mediterranean Coastal Plain. *Earth Planet. Sci.*  
797 *Lett.* **87**, 338–346.
- 798 Bottomley D. ., Ross J. . and Clarke W. . (1984) Helium and neon isotope geochemistry of some  
799 ground waters from the Canadian Precambrian Shield. *Geochim. Cosmochim. Acta* **48**, 1973–  
800 1985.
- 801 Boulton P. J., Johns D. R. and Lang S. C. (2004) Subsurface plumbing of the Crayfish Group in the Penola  
802 Trough: Otway Basin. In *Eastern Australasian Basins Symposium II Petroleum Exploration*  
803 Society of Australia (PESA). pp. 483–498.
- 804 Boyce J. (2013) The Newer Volcanics Province of southeastern Australia: a new classification scheme  
805 and distribution map for eruption centres. *Aust. J. Earth Sci.* **60**, 449–462.
- 806 Bräuer K., Geissler W. H., Kämpf H., Niedermann S. and Rman N. (2016) Helium and carbon isotope  
807 signatures of gas exhalations in the westernmost part of the Pannonian Basin (SE Austria/NE  
808 Slovenia): Evidence for active lithospheric mantle degassing. *Chem. Geol.* **422**, 60–70.
- 809 Caffee, M.W., Hudson, G.B., Velsko, C., Huss, G.R., Alexander, E.C. and Chivas A. R. (1999) Primordial  
810 Noble Gases from Earth's Mantle: Identification of a Primitive Volatile Component. *Science*.  
811 **285**, 2115–2118.
- 812 Cartwright I., Weaver T., Tweed S., Ahearne D., Cooper M., Czapnik K. and Tranter J. (2002) Stable  
813 isotope geochemistry of cold CO<sub>2</sub>-bearing mineral spring waters, Daylesford, Victoria, Australia:  
814 Sources of gas and water and links with waning volcanism. *Chem. Geol.* **185**, 71–91.
- 815 Cas R. A. F., van Otterloo J., Blaikie T. N. and van den Hove J. (2017) The dynamics of a very large  
816 intra-plate continental basaltic volcanic province, the Newer Volcanics Province, SE Australia,  
817 and implications for other provinces. *Geol. Soc. London, Spec. Publ.* **446**, 123–172.
- 818 Cayley R. A., Korsch R. J., Moore D. H., Costelloe R. D., Nakamura A., Willman C. E., Rawling T. J.,  
819 Morand V. J., Skladzien P. B. and O'Shea P. J. (2011) Crustal architecture of central Victoria:  
820 Results from the 2006 deep crustal reflection seismic survey. *Aust. J. Earth Sci.* **58**, 113–156.
- 821 Chivas A. R., Barnes I. E., Lupton J. E. and Collerson K. (1983) Isotopic studies of south-east Australian  
822 CO<sub>2</sub> discharges. *Geol. Soc. Aust. Abstr.* **12**, 94–95.
- 823 Chivas A. R., Barnes I., Evans W. C., Lupton J. E. and Stone J. O. (1987) Liquid carbon dioxide of  
824 magmatic origin and its role in volcanic eruptions. *Nature* **326**, 587–589.

- 825 Clennell M. Ben (1997) Tortuosity: a guide through the maze. *Geol. Soc. London, Spec. Publ.* **122**,  
826 299–344.
- 827 Coulson A. (1933) The older volcanic and Tertiary marine beds at Curlewis, near Geelong. *Proc. R.*  
828 *Soc. Victoria* **45**, 140–149.
- 829 Cox S. F., Sun S. S., Etheridge M. A., Wall V. J. and Potter T. F. (1995) Structural and geochemical  
830 controls on the development of turbidite- hosted gold quartz vein deposits, Wattle Gully mine,  
831 central Victoria, Australia. *Econ. Geol.* **90**, 1722–1746.
- 832 Craig H. (1978) A mantle helium component in circum-Pacific volcanic gases: Hakone, the Marianas  
833 and Mt. Lassen. *Terrestrial Rare Gases*, 3–16.
- 834 Craig H. and Lupton J. E. (1976) Primordial neon, helium, and hydrogen in oceanic basalts. *Earth*  
835 *Planet. Sci. Lett.* **31**, 369–385.
- 836 Crossey L. J., Karlstrom K. E., Springer A. E., Newell D., Hilton D. R. and Fischer T. (2009) Degassing of  
837 mantle-derived CO<sub>2</sub> and He from springs in the southern Colorado Plateau region - Neotectonic  
838 connections and implications for groundwater systems. *Bull. Geol. Soc. Am.* **121**, 1034–1053.
- 839 Crovetto R. (1991) Evaluation of solubility data of the system CO<sub>2</sub>–H<sub>2</sub>O from 273 K to the critical  
840 point of water. *J. Phys. Chem. Ref. Data* **20**, 575–589.
- 841 Crovetto R., Fernández-Prini R. and Japas M. L. (1982) Solubilities of inert gases and methane in H<sub>2</sub>O  
842 and in D<sub>2</sub>O in the temperature range of 300 to 600 K. *J. Chem. Phys.* **76**, 1077–1086.
- 843 Dahlhaus (2003) *The Dell, Clifton Springs. 3-dimensional geological model.*, Available at:  
844 [http://www.ccmaknowledgebase.vic.gov.au/soilhealth/soils\\_resource\\_details.php?resource\\_id](http://www.ccmaknowledgebase.vic.gov.au/soilhealth/soils_resource_details.php?resource_id=2416)  
845 [=2416](http://www.ccmaknowledgebase.vic.gov.au/soilhealth/soils_resource_details.php?resource_id=2416).
- 846 Darrah T. H., Vengosh A., Jackson R. B., Warner N. R. and Poreda R. J. (2014) Noble gases identify the  
847 mechanisms of fugitive gas contamination in drinking-water wells overlying the Marcellus and  
848 Barnett Shales. *Proc. Natl. Acad. Sci.* **111**, 14076–14081.
- 849 Davies D. R. and Rawlinson N. (2014) On the origin of recent intraplate volcanism in Australia.  
850 *Geology* **42**, 1031–1034.
- 851 Deines P., Langmuir D. and Harmon R. S. (1974) Stable carbon isotope ratios and the existence of a  
852 gas phase in the evolution of carbonate ground waters. *Geochim. Cosmochim. Acta* **38**, 1147–  
853 1164.

- 854 Demidjuk Z., Turner S., Sandiford M., George R., Foden J. and Etheridge M. (2007) U-series isotope  
855 and geodynamic constraints on mantle melting processes beneath the Newer Volcanic Province  
856 in South Australia. *Earth Planet. Sci. Lett.* **261**, 517–533.
- 857 Dixon T., McCoy S. T. and Havercroft I. (2015) Legal and regulatory developments on CCS. *Int. J.*  
858 *Greenh. Gas Control* **40**, 431–448.
- 859 Duddy I. R. (1997) Focussing exploration in the Otway Basin: understanding timing of source rock  
860 maturation. *APPEA J.* **37**, 178–191.
- 861 Dunbar E., Cook G. T., Naysmith P., Tripney B. G. and Xu S. (2016) AMS <sup>14</sup>C dating at the Scottish  
862 Universities Environmental Research Centre (SUERC) radiocarbon dating laboratory.  
863 *Radiocarbon* **58**, 9–23.
- 864 Eberhardt P., Eugster O. and Marti K. (1965) A redetermination of the isotopic composition of  
865 atmospheric neon. *Zeitschrift für Naturforsch. A* **20**, 623–624.
- 866 Giese R., Henniges J., Lüth S., Morozova D., Schmidt-Hattenberger C., Würdemann H., Zimmer M.,  
867 Cosma C. and Juhlin C. (2009) Monitoring at the CO<sub>2</sub> SINK site: A concept integrating  
868 geophysics, geochemistry and microbiology. *Energy Procedia* **1**, 2251–2259.
- 869 Giggenbach W. F., Sano Y. and Wakita H. (1993) Isotopic composition of helium, and CO<sub>2</sub> and CH<sub>4</sub>  
870 contents in gases produced along the New Zealand part of a convergent plate boundary.  
871 *Geochim. Cosmochim. Acta* **57**, 3427–3455.
- 872 Gilfillan S., Haszedline S., Stuart F., Gyore D., Kilgallon R. and Wilkinson M. (2014) The application of  
873 noble gases and carbon stable isotopes in tracing the fate, migration and storage of CO<sub>2</sub>.  
874 *Energy Procedia* **63**, 4123–4133.
- 875 Gilfillan S. M. V., Sherk G. W., Poreda R. J. and Haszeldine R. S. (2017) Using noble gas fingerprints at  
876 the Kerr Farm to assess CO<sub>2</sub> leakage allegations linked to the Weyburn-Midale CO<sub>2</sub> monitoring  
877 and storage project. *Int. J. Greenh. Gas Control* **63**, 215–225.
- 878 Gilfillan S. M. V, Ballentine C. J., Holland G., Blagburn D., Lollar B. S., Stevens S., Schoell M. and  
879 Cassidy M. (2008) The noble gas geochemistry of natural CO<sub>2</sub> gas reservoirs from the Colorado  
880 Plateau and Rocky Mountain provinces, USA. *Geochim. Cosmochim. Acta* **72**, 1174–1198.
- 881 Gilfillan S. M. V, Lollar B. S., Holland G., Blagburn D., Stevens S., Schoell M., Cassidy M., Ding Z., Zhou  
882 Z., Lacrampe-Couloume G. and Ballentine C. J. (2009) Solubility trapping in formation water as  
883 dominant CO(2) sink in natural gas fields. *Nature* **458**, 614–618.



- 884 Györe D., Gilfillan S. M. V. and Stuart F. M. (2017) Tracking the interaction between injected CO<sub>2</sub> and  
885 reservoir fluids using noble gas isotopes in an analogue of large-scale carbon capture and  
886 storage. *Appl. Geochemistry* **78**, 116–128.
- 887 Györe D., Stuart F. M., Gilfillan S. M. V and Waldron S. (2015) Tracing injected CO<sub>2</sub> in the Cranfield  
888 enhanced oil recovery field (MS, USA) using He, Ne and Ar isotopes. *Int. J. Greenh. Gas Control*  
889 **42**, 554–561.
- 890 Hand M. and Sandiford M. (1999) Intraplate deformation in central Australia, the link between  
891 subsidence and fault reactivation. *Tectonophysics* **305**, 121–140.
- 892 Haszeldine R. S., Quinn O., England G., Wilkinson M., Shipton Z. K., Evans J. P., Heath J., Crossey L.,  
893 Ballentine C. J. and Graham C. M. (2005) Natural geochemical analogues for carbon dioxide  
894 storage in deep geological porous reservoirs, a United Kingdom perspective. *Oil Gas Sci.*  
895 *Technol.* **60**, 33–49.
- 896 Hilton D. R. (2009) The helium and carbon isotope systematics of a continental geothermal system:  
897 results from monitoring studies at Long Valley caldera (California, U.S.A.). **127**, 1–27.
- 898 Holland G. and Gilfillan S. (2013) Application of noble gases to the viability of CO<sub>2</sub> storage. In *The*  
899 *Noble Gases as Geochemical Tracers*, Springer Berlin Heidelberg, Berlin, Heidelberg. pp. 177–  
900 223.
- 901 Holland G., Lollar B. S., Li L., Lacrampe-Couloume G., Slater G. F. and Ballentine C. J. (2013) Deep  
902 fracture fluids isolated in the crust since the Precambrian era. *Nature* **497**, 357–360.
- 903 IPCC (2005) *IPCC Special Report on Carbon Dioxide Capture and Storage.*, UK: Cambridge University  
904 Press, New York. Available at: [https://www.ipcc.ch/pdf/special-](https://www.ipcc.ch/pdf/special-reports/srccs/srccs_wholereport.pdf)  
905 [reports/srccs/srccs\\_wholereport.pdf](https://www.ipcc.ch/pdf/special-reports/srccs/srccs_wholereport.pdf).
- 906 Italiano F., Yuce G., Uysal I. T., Gasparon M. and Morelli G. (2014) Insights into mantle-type volatiles  
907 contribution from dissolved gases in artesian waters of the Great Artesian Basin, Australia.  
908 *Chem. Geol.* **378–379**, 75–88.
- 909 Jeandel E., Battani A. and Sarda P. (2010) Lessons learned from natural and industrial analogues for  
910 storage of carbon dioxide. *Int. J. Greenh. Gas Control* **4**, 890–909.
- 911 Karolytè R., Serno S., Johnson G. and Gilfillan S. M. V. (2017) The influence of oxygen isotope  
912 exchange between CO<sub>2</sub> and H<sub>2</sub>O in natural CO<sub>2</sub>-rich spring waters: Implications for  
913 geothermometry. *Appl. Geochemistry* **84**, 173–186.

- 914 King S. D. and Anderson D. L. (1998) Edge-driven convection. *Earth Planet. Sci. Lett.* **160**, 289–296.
- 915 Kipfer R., Aeschbach-Hertig W., Peeters F. and Stute M. 4 Noble Gases in Lakes and Ground Waters.
- 916 Kipfer R., Aeschbach-Hertig W., Peeters F. and Stute M. (2002) Noble Gases in Lakes and Ground  
917 Waters. *Rev. Mineral. Geochemistry* **47**, 615–700.
- 918 Lawrence C. R. (1969) Hydrogeology of the Daylesford Mineral District with special reference to the  
919 mineral springs. *Geol. Surv. Victoria, Undergr. water Investig. Rep.* **12**.
- 920 Lee J.-Y., Marti K., Severinghaus J. P., Kawamura K., Yoo H.-S., Lee J. B. and Kim J. S. (2006) A  
921 redetermination of the isotopic abundances of atmospheric Ar. *Geochim. Cosmochim. Acta* **70**,  
922 4507–4512.
- 923 Lesti C., Giordano G., Salvini F. and Cas R. (2008) Volcano tectonic setting of the intraplate, Pliocene-  
924 Holocene, Newer Volcanic Province (southeast Australia): Role of crustal fracture zones. *J.*  
925 *Geophys. Res. Solid Earth* **113**, 1–11.
- 926 Liu W., Tao C., Borjigin T., Wang J., Yang H., Wang P., Luo H. and Zhai C. (2016) Formation time of gas  
927 reservoir constrained by the time-accumulation effect of  $4\text{He}$ : Case study of the Puguang gas  
928 reservoir. *Chem. Geol.* **469**, 246–251.
- 929 Lyon P. J., Boulton P. J., Watson M. N. and Hillis R. (2005) A systematic fault seal evaluation of the  
930 Ladbroke Grove and Pyrus traps of the Penold Trough, Otway Basin. *Aust. Pet. Prod. Explor.*  
931 *Assoc. J.* **45**, 459–476.
- 932 Mao X., Wang Y., Chudaev O. V. and Wang X. (2009) Geochemical evidence of gas sources of  $\text{CO}_2$ -rich  
933 cold springs from Wudalianchi, Northeast China. *J. Earth Sci.* **20**, 959–970.
- 934 Marty B. and Jambon A. (1987)  $\text{C}^3\text{He}$  in volatile fluxes from the solid Earth: implications for carbon  
935 geodynamics. *Earth Planet. Sci. Lett.* **83**, 16–26.
- 936 Marty B. and Tolstikhin I. N. (1998)  $\text{CO}_2$  fluxes from mid-ocean ridges, arcs and plumes. *Chem. Geol.*  
937 **145**, 233–248.
- 938 Matsumoto T., Honda M., McDougall I. and O’reilly S. Y. (1998) Noble gases in anhydrous lherzolites  
939 from the Newer Volcanics, southeastern Australia: A MORB-like reservoir in the subcontinental  
940 mantle.
- 941 Matsumoto T., Honda M., McDougall I., Yatsevich I. and O’reilly S. Y. (1997) Plume-like neon in a  
942 metasomatic apatite from the Australian lithospheric mantle. *Nature* **388**, 162.

- 943 Matsumoto T., Pinti D. L., Matsuda J. and Umino S. (2002) Recycled noble gas and nitrogen in the  
944 subcontinental lithospheric mantle: Implications from N-He-Ar in fluid inclusions of SE  
945 Australian xenoliths. *Geochem. J.* **36**, 209–217.
- 946 Matthews A., Fouillac C., Hill R., O’Nions R. K. and Oxburgh E. R. (1987) Mantle-derived volatiles in  
947 continental crust: the Massif Central of France. *Earth Planet. Sci. Lett.* **85**, 117–128.
- 948 Myers M., Stalker L., Pejcic B. and Ross A. (2013) Tracers – Past, present and future applications in  
949 CO<sub>2</sub> geosequestration. *Appl. Geochemistry* **30**, 125–135.
- 950 Newell D. L., Jessup M. J., Hilton D. R., Shaw C. A. and Hughes C. A. (2015) Mantle-derived helium in  
951 hot springs of the Cordillera Blanca, Peru: Implications for mantle-to-crust fluid transfer in a  
952 flat-slab subduction setting. *Chem. Geol.* **417**, 200–209.
- 953 O’Nions R. K. and Oxburgh E. R. (1988) Helium, volatile fluxes and the development of continental  
954 crust. *Earth Planet. Sci. Lett.* **90**, 331–347.
- 955 Ozima M. and Podosek F. A. (2002) *Noble Gas Geochemistry.*, Cambridge University Press.
- 956 Price R. C., Gray C. M. and Frey F. A. (1997) Strontium isotopic and trace element heterogeneity in  
957 the plains basalts of the Newer Volcanic Province, Victoria, Australia. *Geochim. Cosmochim.*  
958 *Acta* **61**, 171–192.
- 959 Roberts J. J., Gilfillan S. M. V., Stalker L. and Naylor M. (2017) Geochemical tracers for monitoring  
960 offshore CO<sub>2</sub> stores. *Int. J. Greenh. Gas Control* **65**, 218–234.
- 961 Roberts J. J., Leplastrier A., Feitz A. J., Shipton Z. K., Bell A. F. and Karolytè R. (2019) Structural  
962 controls on the location and distribution of CO<sub>2</sub> emission at a natural CO<sub>2</sub> spring in Daylesford,  
963 Australia. *Int. J. Greenh. Gas Control* **84**, 36–46.
- 964 Robertson G. B., Prescott J. R. and Hutton J. T. (1996) Thermoluminescence dating of volcanic activity  
965 at Mount Gambier, South Australia. *Trans. R. Soc. South Aust.* **120**, 7–12.
- 966 Rudnick R. L. and Fountain D. M. (1995) Nature and composition of the continental crust: A lower-  
967 crustal perspective. *Rev. Geophys.* **33**, 267–309.
- 968 Ruzié L., Aubaud C., Moreira M., Agrinier P., Dessert C., Gréau C. and Crispi O. (2013) Carbon and  
969 helium isotopes in thermal springs of La Soufrière volcano (Guadeloupe, Lesser Antilles):  
970 Implications for volcanological monitoring. *Chem. Geol.* **359**, 70–80.
- 971 Sakamoto M., Sano Y. and Wakita H. (1992) <sup>3</sup>He/<sup>4</sup>He ratio distribution in and around the Hakone

- 972 volcano. *Geochem. J.* **26**, 189–195.
- 973 Sano Y. and Marty B. (1995) Origin of carbon in fumarolic gas from island arcs. *Chem. Geol.* **119**, 265–  
974 274.
- 975 Sano Y., Takahata N. and Seno T. (2006) Geographical distribution of  $^3\text{He}/^4\text{He}$  ratios in the Chugoku  
976 District, Southwestern Japan. *Pure Appl. Geophys.* **163**, 745–757.
- 977 Sano Y., Wakita H. and Williams S. N. (1990) Helium-isotope systematics at Nevado del Ruiz volcano,  
978 Colombia: implications for the volcanic hydrothermal system. *J. Volcanol. Geotherm. Res.* **42**,  
979 41–52.
- 980 Sherwood Lollar B., Ballentine C. J. and O’Nions R. K. (1997) The fate of mantle-derived carbon in a  
981 continental sedimentary basin: Integration of relationships and stable isotope signatures.  
982 *Geochim. Cosmochim. Acta* **61**, 2295–2307.
- 983 Sherwood Lollar B., O’Nions R. K. and Ballentine C. J. (1994) Helium and neon isotope systematics in  
984 carbon dioxide-rich and hydrocarbon-rich gas reservoirs. *Geochim. Cosmochim. Acta* **58**, 5279–  
985 5290.
- 986 Shugg A. (2009) Hepburn Spa: Cold carbonated mineral waters of Central Victoria, South Eastern  
987 Australia. *Environ. Geol.* **58**, 1663–1673.
- 988 Smith S. P. (1985) Noble gas solubility in water at high temperature. *Eos (Washington, DC)*. **66**, 397.
- 989 Stalker L. and Myers M. (2014) Tracers—pilot versus commercial scale deployment for carbon  
990 storage. *Energy Procedia* **63**, 4199–4208.
- 991 Teasdale J. P., Pryer L. L., Stuart-Smith P. G., Romine K. K., Etheridge M. A., Loutit T. S. and Kyan D.  
992 M. (2003) Structural framework and basin evolution of Australia’s southern margin. *APPEA J.*  
993 **43**, 13–37.
- 994 Tolstikhin I. N., Ballentine C. J., Polyak B. G., Prasolov E. M. and Kikvadze O. E. (2017) The noble gas  
995 isotope record of hydrocarbon field formation time scales. *Chem. Geol.* **471**, 141–152.
- 996 Torgersen T. (1980) Controls on pore-fluid concentration of  $^4\text{He}$  and  $^{222}\text{Rn}$  and the calculation of  
997  $^4\text{He}/^{222}\text{Rn}$  ages. *J. Geochemical Explor.* **13**, 57–75.
- 998 van Otterloo J., Cas R. A. F. and Sheard M. J. (2013) Eruption processes and deposit characteristics at  
999 the monogenetic Mt. Gambier Volcanic Complex, SE Australia: implications for alternating  
1000 magmatic and phreatomagmatic activity. *Bull. Volcanol.* **75**, 737.

- 1001 van Otterloo J., Raveggi M., Cas R. A. F. and Maas R. (2014) Polymagmatic activity at the  
1002 monogenetic Mt Gambier Volcanic Complex in the Newer Volcanics Province, SE Australia: New  
1003 insights into the occurrence of intraplate volcanic activity in Australia. *J. Petrol.* **55**, 1317–1351.
- 1004 Walton N. R. G. (1989) Electrical conductivity and Total Dissolved Solids—what is their precise  
1005 relationship? *Desalination* **72**, 275–292.
- 1006 Warr O., Sherwood Lollar B., Fellowes J., Sutcliffe C. N., McDermott J. M., Holland G., Mabry J. C. and  
1007 Ballentine C. J. (2018) Tracing ancient hydrogeological fracture network age and  
1008 compartmentalisation using noble gases. *Geochim. Cosmochim. Acta* **222**, 340–362.
- 1009 Watson M. N., Boreham C. J. and Tingate P. R. (2004) Carbon dioxide and carbonate cements in the  
1010 Otway Basin; implications for geological storage of carbon dioxide. *APPEA J.* **44**, 703–720.
- 1011 Watson M. N., Zwingmann N., Lemon N. M. and Tingate P. R. (2003) Onshore Otway Basin carbon  
1012 dioxide accumulations: CO<sub>2</sub>-induced diagenesis in natural analogues for underground storage  
1013 of greenhouse gas. *APPEA J.* **43**, 637–653.
- 1014 Weast R. C., Astle M. J. and Beyer W. H. (1988) *CRC Handbook of Chemistry and Physics.*, CRC press  
1015 Boca Raton, FL.
- 1016 Weinlich F. H., Bräuer K., Kämpf H., Strauch G., Tesař J. and Weise S. M. (1999) An active  
1017 subcontinental mantle volatile system in the western Eger rift, Central Europe: Gas flux,  
1018 isotopic (He, C, and N) and compositional fingerprints. *Geochim. Cosmochim. Acta* **63**, 3653–  
1019 3671.
- 1020 Wellman P. (1983) Hotspot volcanism in Australia and New Zealand: Cainozoic and mid-Mesozoic.  
1021 *Tectonophysics* **96**, 225–243.
- 1022 Wellman P. and McDougall I. (1974) Cainozoic igneous activity in eastern Australia. *Tectonophysics*  
1023 **23**, 49–65.
- 1024 Wilkinson M., Gilfillan S. M. V, Haszeldine R. S. and Ballentine C. J. (2009) Plumbing the Depths:  
1025 Testing Natural Tracers of Subsurface CO<sub>2</sub> Origin and Migration, Utah. In *Carbon dioxide*  
1026 *sequestration in geological media-State of the science* AAPG Special Volumes. pp. 619–634.
- 1027 Williams S. N., Sano Y. and Wakita H. (1987) Helium-3 emission from Nevado Del Ruiz Volcano,  
1028 Colombia. *Geophys. Res. Lett.* **14**, 1035–1038.
- 1029 Wycherley H., Fleet A. and Shaw H. (1999) Some observations on the origins of large volumes of

- 1030 carbon dioxide accumulations in sedimentary basins. *Mar. Pet. Geol.* **16**, 489–494.
- 1031 Zartman R. E., Wasserburg G. J. and Reynolds J. H. (1961) Helium, argon, and carbon in some natural  
1032 gases. *J. Geophys. Res.* **66**, 277–306.
- 1033 Zhou Z. and Ballentine C. J. (2006)  $^4\text{He}$  dating of groundwater associated with hydrocarbon  
1034 reservoirs. *Chem. Geol.* **226**, 309–327.